REVIEW

EcoMat
FUNCTIONAL MATERIALS FOR GREEN ENERGY AND ENVIRONMENT    WILEY

# Zinc based micro-electrochemical energy storage devices: Present status and future perspective

Xiao Wang[1,2,3]  |  Zhong-Shuai Wu[1,2]

[1]State Key Laboratory of Catalysis, Dalian Institute of Chemical Physics, Chinese Academy of Sciences, Dalian, China

[2]Dalian National Laboratory for Clean Energy, Chinese Academy of Sciences, Dalian, China

[3]University of Chinese Academy of Sciences, Beijing, China

**Correspondence**
Zhong-Shuai Wu, Dalian National Laboratory for Clean Energy, Dalian Institute of Chemical Physics, Chinese Academy of Sciences, 457 Zhongshan Road, Dalian 116023, China.
Email: wuzs@dicp.ac.cn

**Abstract**

In order to keep rapid pace with increasing demand of wearable and miniature electronics, zinc-based microelectrochemical energy storage devices (MESDs), as a promising candidate, have gained increasing attention attributed to low cost, environmental benign, and high performance. Herein, this review summarizes the state-of-the-art advances of zinc-based MESDs in microbatteries (MBs) and microsupercapacitors and highlights merits of cost effectiveness and high performance for miniaturized smart integrated systems. First, an introduction is given to present importance of zinc-based MESDs. Second, current status with representative fiber, in-plane and sandwiched configurations are illustrated in detail, particularly with a focus on the reasonable construction of multifunctional MBs and microsupercapacitors and deep understanding of energy storage mechanisms. Then, achievements for smart systems are overviewed to highlight environmental adaptability, integratable properties, and scalability in targeting applications. Finally, critical perspectives and challenges on the synergistic optimization of whole device are discussed to demonstrate forward-looking developmental directions of zinc-based MESDs.

**KEYWORDS**

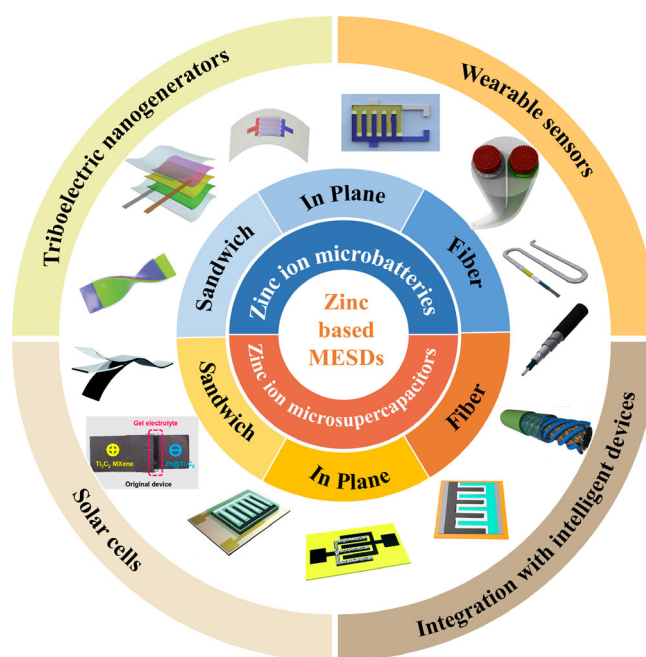microbatteries, microelectrochemical energy storage devices, microsupercapacitors, zinc ion

# 1 | INTRODUCTION

The booming development of microelectrochemical energy storage devices (MESDs) is driven by the smart, wearable, and flexible microelectronics applied in microrobots, wireless self-powered systems, patient tracking and location, implantable medical sensors, and internet of things.[1-3] However, current power sources with heavy mass, undesired big volume, and inferior flexibility cannot satisfy the demand of MESDs with the compatible advantages of light weight, miniaturization, tunable thinness, and mechanical flexibility.[4] To provide a microscale power source for these intelligent applications, MESDs delivering high volumetric energy density are especially indispensable since there is stringent size constrains for the integration with other electronics. In principle, the total areal size of MESDs could be in the millimeter or even in the centimeter scale with different configurations.[5] To date, lithium-based MESDs, especially for lithium thin-film microbatteries (MBs) (<1 mm in thickness),[3,6-8] have been extensively developed in commercial application for wearable and card-type devices. Nevertheless, these lithium thin-film MBs exhibit low volumetric energy densities (<200 Wh/L), comparing with conventional sandwich lithium-ion batteries (<650 Wh/L).[9] Furthermore, high cost of the scarce raw material, toxic and flammable electrolyte, rigorous assembly condition with glovebox, and easy leaking of the electrolyte impede the widespread application of the lithium-based MESDs with the utilization in implantable, wearable, and flexible applications that tightly touch with human body.[10] As a result, the "beyond lithium-based" MESDs with form factors such as highly safe, low cost, miniaturized, versatile, intelligent, and integrated features have attracted incremental attention.

As attractive alternatives for lithium-based MESDs, zinc-based MESDs with great potential to produce high volumetric capacity utilizing environmentally friendly raw materials have captured increasing attentions, due to the abundant reserves, low cost, high safety in aqueous electrolyte, and easy processing.[11-14] Moreover, comparing with the single-electron transfer of lithium-based MESDs, zinc-based MESDs employ the two-electron transfer during the charging and discharging process, which can deliver both high gravimetric capacity (820 mAh/g) and high volumetric capacity (5855 mAh/cm$^3$).[15] It is noteworthy that the aqueous electrolyte of zinc-based MESDs not only provides faster ion diffusion than the nonaqueous electrolyte in lithium-based MESDs, but also guarantees outstanding safety of the microdevices.[16] Moreover, the high redox potential of the zinc anode (−0.763 V vs standard hydrogen electrode) allows zinc-based MESDs to stably work in aqueous electrolyte,

which is difficult to be fulfilled for lithium-based MESDs.[17] Notably, the reversibility of zinc insertion/extraction in near-neutral or mild acidic electrolyte (e.g., pH = 3.6-6.0) protects the zinc anode from the formation of zinc dendrites and other byproducts.[18,19] Taking into consideration of the above, it is anticipated that zinc-based MESDs are very promise for the safe and wearable electronics applications towards high-performance, miniaturization, flexibility, integration and adaptability.

As is well-known, zinc ion MBs (ZIMBs) and zinc ion microsupercapacitors (ZIMSCs) are the two main zinc-based MESDs as power supplies coupled with various microelectronics.[20-23] As a rule, ZIMBs display high energy density through slow redox reactions, for example, ion insertion/extraction and conversion reaction in the internal electrode, while ZIMSCs through rapid Faradic reaction at the interface between the electrode and electrolyte or the fast adsorption/desorption of electrolyte ions, equipped with high power density.[3,24-26] Compared with ZIMBs, ZIMSCs have come into their renaissance owing to long service life and high power density.[5] To this end, we systematically summarize the recent advances of zinc-based MESDs in ZIMBs and ZIMSCs for their intelligent integrated systems (Figure 1). First, a timeline of the development of ZIMBs is given to introduce the history of ZIMBs. Second, the state-of-the-art achievements of both ZIMBs and ZIMSCs with different configurations in fiber, in-plane, and sandwiched types are presented for their integrated systems, such as



**FIGURE 1** Schematic of zinc-based microelectrochemical energy storage devices (MESDs) with different configurations for intelligent integrated systems

smart watch, mobile phone, smart insole, and wearable fabrics. As an emphasis, the integration with other intelligent systems are overviewed for further understanding and exploiting their potential value. Finally, the key challenges, prospects, and future developments of zinc-based MESDs are briefly discussed for their applications in smart microelectronics.

## 2 | ZINC ION MBs

In the last decade, ZIMBs have been boomed with diversified configurations and cathodes, due to their intrinsic virtues of exceptional safety and high energy density.[1] The development of ZIMBs from the conventional primary planar MBs to various configuration rechargeable MBs is summarized in Figure 2. It can be seen that, since the first employment of the metallic zinc in 1799, zinc anode has always been a conspicuous negative electrode in the primary and secondary batteries attributed to high theoretical capacity and relatively low redox potential.[14,48] At the beginning, zinc anode was widely explored in alkaline Zn-MnO$_2$ primary MBs,[27,28,35] Zn-Ni MBs,[44] and Zn-Ag MBs.[29,37] Ascribed to the irreversible discharge products and limited rechargeability, Yamamoto et al. in 1986,[49] firstly replaced the alkaline electrolyte in the primary batteries with the mild neutral zinc sulfate electrolyte, but the fundamental mechanism was still far from clear. After that, aqueous ZIMBs were developed rapidly with differently innovative configuration of fiber, interdigital, and sandwich, targeting for smart, portable, and wearable electronics. To clearly overview the development in this filed, we made a systematical summary of various ZIMBs with representative configurations (e.g., fiber, sandwich, and in-plane) and various performance metrics, as listed in Table 1.
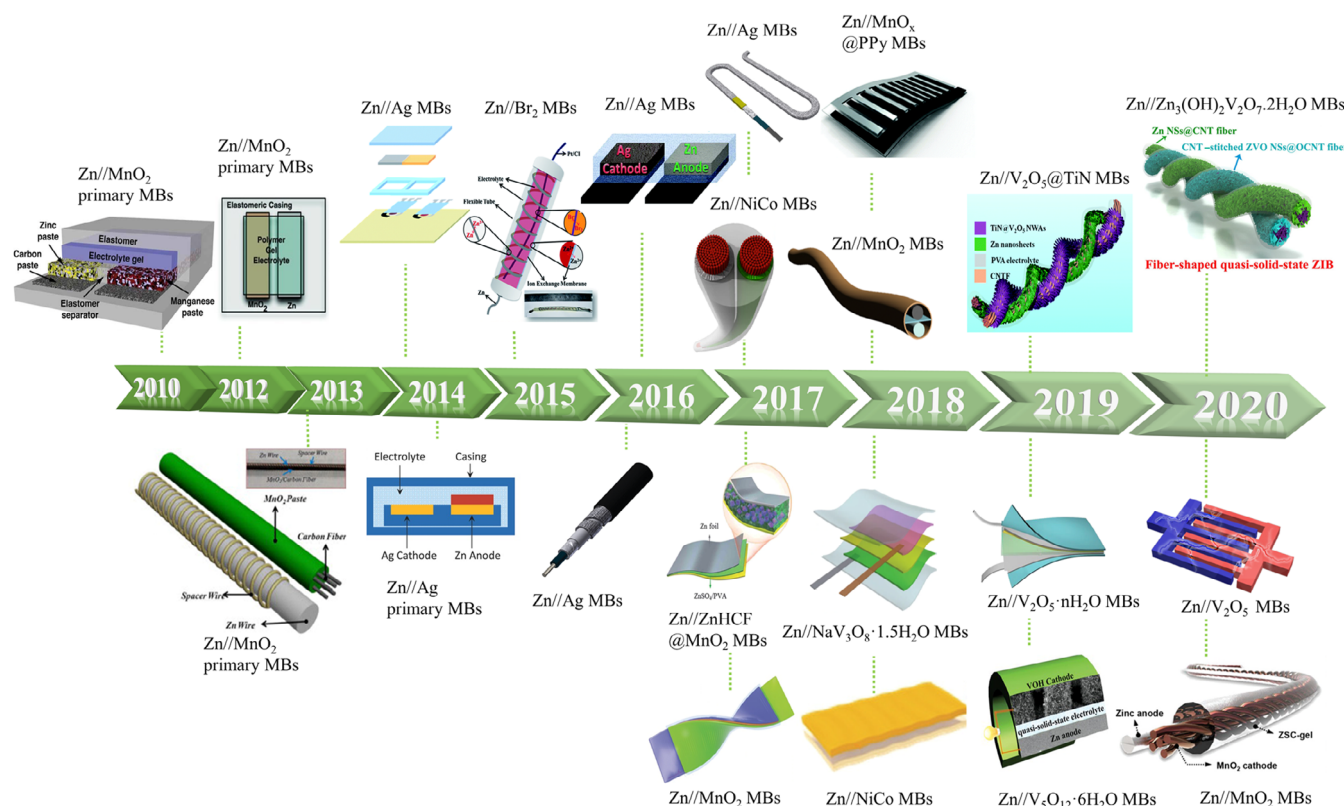


**FIGURE 2** Timeline of the development of ZIMBs. Images reproduced with permission as follows: "Zn//MnO$_2$ primary MBs," "Zn//Ag primary MBs," "Zn//Ag MBs," "Zn//MnO$_2$ MBs," "Zn//NiCo MBs," "Zn//V$_5$O$_{12}$·6H$_2$O MBs," and "Zn//V$_2$O$_5$ MBs," reproduced with permission.[27-34] Copyright 2010, 2012, 2014, 2016, 2017, 2018, 2019, and 2020, Wiley-VCH. "Zn//MnO$_2$ primary MBs" and "Zn//V$_2$O$_5$·nH$_2$O MBs," reproduced with permission.[35,36] Copyright 2013 and 2019, Elsevier. "Zn//Ag MBs," "Zn//Br$_2$ MBs," "Zn//ZnHCF@MnO$_2$ MBs," "Zn//MnO$_x$@PPy MBs," and "Zn//V$_2$O$_5$@TiN MBs," reproduced with permission.[37-42] Copyright 2014, 2015, 2016, 2017, 2018, and 2019, Royal Society of Chemistry. "Zn//Ag MBs," reproduced with permission.[43] Copyright 2017, American Association for the Advancement of Science. "Zn//NiCo MBs," "Zn//MnO$_2$ MBs," and "Zn//Zn$_3$(OH)$_2$V$_2$O$_7$·2H$_2$O MBs," reproduced with permission.[44-46] Copyright 2017, 2018, and 2020, American Chemical Society. "Zn//NaV$_3$O$_8$·1.5H$_2$O MBs," reproduced with permission.[47] Copyright 2018, Nature Publishing Group. MBs, microbatteries; ZIMBs, zinc ion MBs

**TABLE 1** Performance comparison of the state-of-the-art ZIMBs with different configurations

| Configuration type | | Electrode | Working potential (V) | Electrolyte | Capacity | Capacity retention (%)/cycle number | Energy density | Power density | Refs. |
|---|---|---|---|---|---|---|---|---|---|
| Fiber | Parallel | Zn//MnO$_2$@carbon[a] | 0.8-1.5 | 6 M NH$_4$Cl 0.8 M ZnCl$_2$ | 0.15 mAh/cm at 0.15 mA | Not rechargeable | - | - | 35 |
| Fiber | Parallel | Zn//MnO$_2$@CNT[b] | 1.0-1.8 | PVA-1.5 M LiCl-2 M ZnCl$_2$ | 290 mAh/g at 0.1 A/g | 75%/300 | 360 Wh/Kg | 100 W/Kg | 45 |
| Fiber | Parallel | Zn//MnO$_2$ | 1.0-2.0 | PAM-2 M ZnSO$_4$-0.1 M MnSO$_4$ | 302.1 mAh/g at 60 mA/g | 98.5%/500 | 53.8 mWh/cm$^3$ | - | 50 |
| Fiber | Parallel | Zn//NCHO[c] | 1.2-2.0 | PVA-KOH-Zn (CH$_3$COO)$_2$ | 5 mAh/cm$^3$ at 232 C | 60%/1000 | 0.12 mWh/cm$^2$ 8 mWh/cm$^3$ | 32.8 mW/cm$^2$ 2.2 mW/cm$^3$ | 44 |
| Fiber | Parallel | CC-ZnO@C-Zn//CC-CCH@CMO[d] | 1.0-2.0 | PVA-6 M KOH | 3 mAh/cm$^3$ at 25 mA cm$^3$ | 82%/1600 | 4.6 mWh/cm$^3$ | 0.42 W/cm$^3$ | 51 |
| Fiber | Parallel | Zn//Co$_3$O$_4$ | 1.35-2.0 | 1 M KOH-0.01 M Zn(CH$_3$COO)$_2$ | 21.3 mAh/cm$^3$ at 0.25 A/cm$^3$ | 90%/2000 | 5.63 mWh/cm$^3$ 72.5 µWh/cm$^2$ | - | 52 |
| Fiber | Quasi-parallel | Zn//Br$_2$ | 1.2-2.2 | 1 M ZnBr$_2$ | 19 mAh/mL at 22.22 mA/mL | 99%/70 | - | - | 38 |
| Fiber | Twisted | Zn//Ag | 1.0-1.8 | PVA-3 M KOH | 0.276 mAh/mL at 0.1 mA/cm | 52%/3 | - | - | 53 |
| Fiber | Twisted | Zn//Ag$_2$O | 1.2-1.8 | PVA-1 M KOH | 1.05 mAh/cm$^3$ at 0.5 mA/cm$^2$ | 79.5%/200 | 1.57 mWh/cm$^2$ | 14.4 mW/cm$^2$ | 54 |
| Fiber | Twisted | Zn//Ni-NiO | 1.5-2.0 | PVA-4 M KOH-2 M ZnO | 237.8 µAh/cm$^3$ at 3.7 A/g[e] | 96.6%/10 000 | 6.6 µWh/cm$^2$ | 20.2 mW/cm$^2$ | 55 |
| Fiber | Twisted | Zn//Ni | 1.0-2.0 | PVA-2 M KOH-0.08 M ZnSO$_4$ | 19.6 mAh/cm$^3$ at 1.4 A/cm$^3$ | 95%/20 000 | 34 mWh/cm$^3$ | 17.5 W/cm$^3$ | 56 |
| Fiber | Twisted | Zn//MnO$_2$ | 0.8-1.85 | Gelatin-1 M ZnSO$_4$-0.1 M MnSO$_4$ | 174.2 mAh/g at 0.5 C | 60%/1000 | - | - | 57 |
| Fiber | Twisted | Zn//V$_2$O$_5$@N-doped carbon | 0.3-1.6 | PVA-2 M ZnCl$_2$ | 457.5 mAh/cm$^3$ at 0.3 A/cm$^3$ | 85.3%/400 | 85.8 mWh/cm$^3$ | 5.6 W/cm$^3$ | 58 |
| Fiber | Twisted | Zn//TiN@V$_2$O$_5$ | 0-1.6 | PVA-2 M ZnSO$_4$ | 405 mAh/cm$^3$ at 0.5 mA/cm$^2$ | 90.6%/3500 | 283.5 mWh/cm$^3$ | 133.3 mW/cm$^3$ | 42 |
| Fiber | Coaxial | Zn//Ag | 1.0-1.8 | PVA-2 M KOH-0.2 M ZnO (saturated Bi$_2$O$_3$) | 1.4 mAh/cm at 0.5 C | 98%/170 | - | - | 30 |
| Fiber | Coaxial | Zn//Ag | 1.0-1.8 | PVA-2 M KOH-0.2 M ZnO (saturated Bi$_2$O$_3$) | 1.25 mAh/cm at 0.5 C | 94%/100 | - | - | 43 |

**TABLE 1** (Continued)

| Configuration type | Electrode | Working potential (V) | Electrolyte | Capacity | Capacity retention (%)/ cycle number | Energy density | Power density | Refs. |
|---|---|---|---|---|---|---|---|---|
| Fiber Coaxial | Zn//PANI | 0.5-1.5 | PVA/1 M Zn(CF$_3$SO$_3$)$_2$ | 106 mAh/g at 0.5 A/g | 91.5%/200 | - | - | 59 |
| Fiber Coaxial | Zn//MnO$_2$ | 1.0-1.8 | PVA-3 MLiCl-2 M ZnCl$_2$-0.3 M MnSO$_4$ | 12.86 mAh/cm$^3$ at 20 mA/cm$^3$ | 90.3%/300 | 17.9 mWh/cm$^3$ | 28.1 mW/cm$^3$ | 60 |
| Fiber Coaxial | Zn//ZnHCF$^f$ | 1.0-2.4 | CMC$^g$-0.5 M Zn$_2$SO$_4$ | 100.2 mAh/cm$^3$ at 0.1 A/cm$^3$ | 91.8%/200 | 195.39 mWh/cm$^3$ | 1.9 W/cm$^3$ | 61 |
| Fiber Coaxial | Zn//CoFe(CN)$_6$ | 0.7-2.0 | PAM-F77-4 M Zn(CF$_3$SO$_3$)$_2$ | 171.64 mAh/g at 0.2 A/g | 93.4%/2000 | - | - | 62 |
| Sandwich | Zn//MnO$_2$ | 1.0-2.0 | PVDF-HFP-Zn$^+$Tf$^-$-EMIM$^+$Tf$^-$ | 0.98 mAh/cm$^2$ | - | 1.2 mWh/cm$^2$ | - | 63 |
| Sandwich | Zn//MnO$_2$ | 0.7-1.6 | PAA$^h$-KOH-ZnO | 5.6 mAh/cm$^2$ at 0.5 mA | Not rechargeable | - | - | 64 |
| Sandwich | Zn//MnO$_2$@PEDOT$^i$ | 1.0-1.8 | PVA-ZnCl$_2$/-MnSO$_4$ | 282.4 mAh/g at 2 mA/cm$^2$ | 83.7%/300 | 504.9 Wh/kg (33.95 mWh/cm$^3$) | 8.6 kW/kg | 31 |
| Sandwich | Zn//MnO$_2$ | 0.9-1.8 | PNA$^j$-0.3 M ZnSO$_4$-0.015 M MnSO$_4$ | 145 mAh/g at 0.1 A/g | 167%/600 | - | - | 65 |
| Sandwich | Zn//MnO$_2$ | 1.0-1.8 | Gelatine-ZnSO$_4$-MnSO$_4$ | 139 mAh/g at 1 C | 91%/1000 | 12 mWh/cm$^3$ | 13 mW/cm$^3$ | 66 |
| Sandwich | Zn//MnO$_2$ | 0.9-1.9 | EG-waPUA-PAM-2 M ZnSO$_4$-0.1 M MnSO$_4$ | 226 mAh/g at 0.2 A/g | 87.41%/600 | 32.68 mWh/cm$^3$ | - | 67 |
| Sandwich | Zn//MnO$_2$ | 0.9-2.0 | PAM-ZnSO$_4$-MnSO$_4$ | 306 mAh/g at 61.6 mA/g | 97%/1000 | 6.18 mWh/cm$^2$ | 148.2 mW/cm$^2$ | 68 |
| Sandwich | Zn// ZnHCF$^k$@MnO$_2$ | 1.4-1.9 | PVA-ZnSO$_4$ | 89 mAh/g at 100 mA/g | 71%/500 | 149 Wh/kg | 167 W/kg | 40 |
| Sandwich | Zn//Co$_3$O$_4$ | 1.4-1.93 | PVA-PAA-1 M KOH-0.01 M Zn(CH$_3$COO)$_2$ | 162 mAh/g at 1 A/g | 80%/2000 | 241 Wh/kg | - | 69 |
| Sandwich | Zn//Co$_3$O$_4$ | 0.8-2.3 | PAM-2 M ZnSO$_4$-0.2 M CoSO$_4$ | 52 mAh/g at 8 A/g | 94.6%/2000 | 360.8 Wh/kg | - | 18 |
| Sandwich | Zn//NiCo | 1.2-2.0 | PANa$^l$-0.2 M Zn(CH$_3$COO)$_2$-6 M KOH | 259 mAh/g at 5.8 C | 65%/16 000 | - | - | 70 |

(Continues)

**TABLE 1** (Continued)

| Configuration type | Electrode | Working potential (V) | Electrolyte | Capacity | Capacity retention (%)/ cycle number | Energy density | Power density | Refs. |
|---|---|---|---|---|---|---|---|---|
| Sandwich | Zn//NiCo | 1.2-1.95 | PANa-Fe$^{3+}$-0.2 M Zn(CH$_3$COO)$_2$-6 M KOH | 250 mAh/g at 5C | - | - | - | 32 |
| Sandwich | Zn//Ni | 1.4-1.9 | PVA-KOH | ~200 mAh/g at 7.5 A/g | 94%/2000 | 15 mWh/cm$^3$ | 15 mW/cm$^3$ | 66 |
| Sandwich | Zn//NaV$_3$O$_8$·1.5H$_2$O (NVO) | 0.3-1.3 | Gelatin-1 M ZnSO$_4$ | 288 mAh/g at 0.1 A/g | 85%/90 | 180 Wh/kg | 2160 W/kg | 47 |
| Sandwich | Zn//Co$_{0.247}$V$_2$O$_5$·0.944H$_2$O | 0.5-2.3 | PAM-20 M LiTFSI-1 M Zn(TFSI)$_2$ | 432 mAh/g at 0.1 A/g | 90.26%/7500 | 432 Wh/kg | 25.59 kW/kg | 71 |
| Sandwich | Zn//V$_5$O$_{12}$·6H$_2$O | 0.2-1.6 | Gelatin-3 M Zn(CF$_3$SO$_3$)$_2$ | 300 mAh/g at 0.1 A/g | 96%/50 (bending) | - | - | 33 |
| Sandwich | Zn//V$_2$O$_5$·nH$_2$O | 0.4-1.6 | Gelatin-1 M Zn(CF$_3$SO$_3$)$_2$ | 361 mAh/g at 0.1 A/g | 85%/300 | - | - | 36 |
| Sandwich | Zn//MoS$_2$ | 0.3-1.5 | PAM-2 M ZnSO$_4$ | 199.3 mAh/g at 0.1 A/g | 97.7%/500 | 148.2 Wh/kg | 70.5 W/kg | 72 |
| Sandwich | Zn//FeHCF$^m$ | 0.01-2.3 | PAM-21 M LiTFSI-1 M Zn(TFSI)$_2$ | 76 mAh/g at 8 A/g | 98%/100 (−15°C) | 81.7 Wh/kg | - | 73 |
| In-plane | Zn//Ag | 0.8-2.05 | PAA-6 M KOH-1 M LiOH | 1.3-2.1 mAh/cm$^2$ at 1.4 mA/cm$^2$ | 34%/13 | - | - | 37 |
| In-plane | Zn//Ag | 1.0-2.3 | 1 M ZnSO$_4$-2 M KCl | 0.27 mAh/cm$^2$ at 1 mA/cm$^2$ | ~100%/1000 | 0.44 mWh/cm$^2$ | - | 29 |
| In-plane | Zn//Ag | 0.8-2.1 | PAA-6 M KOH-1 M LiOH | 1.2 mAh/cm$^2$ at 4 mA/cm$^2$ | ~100%/50 | - | 5 mW/cm$^2$ | 39 |
| In-plane | Zn//Ag$_2$O | 0.8-2.3 | PAA-6 M KOH-1 M LiOH | 3 mAh/cm$^2$ at 3 mA/cm$^2$ | ~85%/30 | - | - | 74 |
| In-plane | Zn//LiMn$_2$O$_4$ | 1.4-2.0 | PHE$^n$-0.25 M ZnSO$_4$-0.25 M Li$_2$SO$_4$ | 71.1 mAh/g at 20 mA/ g | 83%/300 | - | - | 75 |
| In-plane | Zn//LiFePO$_4$ | 0.8-1.8 | PHE$^n$-0.25 M ZnSO$_4$-0.25 M Li$_2$SO$_4$ | 168 mAh/g at 1C | 90%/300 | - | - | 75 |
| In-plane | Zn//MnO$_2$ | OCV-1.5 V | NH$_4$Cl-ZnCl$_2$ | 3.5 mAh/cm$^2$ | Not rechargeable | - | - | 27 |
| In-plane | Zn//MnO$_2$ | OCV-1.5 V | PAA-6 M KOH (ZnO) | 3.875 mAh/cm$^2$ | Not rechargeable | - | - | 28 |
| In-plane | Zn//MnO$_2$ | 1-1.9 | 2 M ZnSO$_4$-0.2 M MnSO$_4$ | 53.5 µAh/cm$^2$·µm at 1C | 81.5%/1000 | 71.3 µWh/cm$^2$·µm | 1621.4 µW/cm$^2$·µm | 41 |
| In-plane | Zn//MnO$_2$ | 0.4-1.4 | PAA-based gel | 3.6 mAh/cm$^2$ | Not rechargeable | - | - | 76 |

**TABLE 1** (Continued)

| Configuration type | Electrode | Working potential (V) | Electrolyte | Capacity | Capacity retention (%)/ cycle number | Energy density | Power density | Refs. |
|---|---|---|---|---|---|---|---|---|
| In-plane | $Zn//MnO_2$ | 0.6-1.5 | Gelatin-1 M $ZnSO_4$ | 110 $\mu Ah/cm^2$ at 0.2 $mA/cm^2$ | ~100%/200 | 21 $mWh/cm^3$ | 33 $mW/cm^3$ | 77 |
| In-plane | $Zn//MnO_2$ | 0.9-1.8 | 2 M $ZnSO_4$-0.5 M $MnSO_4$ | 19.3 $mAh/cm^3$ at 7.5 $mA/cm^2$ | ~83.9%/1300 | 17.4 $mWh/cm^3$ | 150 $mW/cm^3$ | 11 |
| In-plane | $Zn//VO_2(B)$ | 0.01-2.0 | PVA-2 M $Zn(CF_3SO_3)_2$ | 314.7 $\mu Ah/cm^2$ at 0.14 $mA/cm^2$ | 71.8%/200 | 188.8 $\mu Wh/cm^2$ | 0.61 $mW/cm^2$ | 78 |

Abbreviations: CNT, carbon nanotube; CMO, CoMoO4; EG-waPUA, EG based waterborne anionic polyurethane acrylates; EMIM+Tf-, 1-butyl-3-methylimidazolium trifluoromethanesulfonate; PAA, polyacrylic acid; PAM, polyacrylamide; PEDOT, poly (3,4-ethylenedioxythiophene); PVA, poly(vinyl alcohol); PVDF-HFP, poly(vinylidene fluoride-hexafluoropropylene); ZIMBs, zinc ion microbatteries.

[a]These batteries belong to primary batteries.
[b]Carbon nanotubes.
[c]Nickel cobalt hydroxide nanosheets.
[d]Carbon cloth-ZnO@C-Zn//carbon-cloth $Co(CO_3)_{0.5}(OH)_x \cdot 0.11H_2O@CoMoO_4$.
[e]Polyurethane acrylates/polyacrylamide.
[f]Zinc hexacyanoferrate.
[g]Carboxymethyl cellulose sodium.
[h]Polyacrylic acid.
[i]Poly(3,4-ethylenedioxythiophene).
[j]Poly(N-isopropylacrylamide-co-acrylic acid)
[k]Zinc hexacyanoferrate.
[l]Sodium polyacrylate hydrogel.
[m]Cyanogroup iron hexacyanoferrate.
[n]Pluronic hydrogel electrolytes (PHEs): adjusting mass of Pluronic polymer and aqueous electrolytes.

## 2.1 | Fiber-type zinc ion MBs

So far, fiber-type ZIMBs are classified into three categories in terms of device configurations, containing parallel, twisted, and coaxial, which have been generally accepted for assembling fiber microdevices.[23] First, the parallel configuration is established with pairing anode and cathode in parallel with a separator separated them. Remarkably, the rigid encapsulation is specially required for impeding the leakage when the electrolyte is liquid. Second, the twisted configuration is assembled with twisting the anode and cathode through a rotation-translation setup, followed by the surface coating of a solid-state electrolyte on electrodes to hinder from short circuits. Ascribed to the similar structure of fabric filaments, this configuration makes them appear to be extremely suitable for wearable applications and scale-up energy textiles only if the twisted fibers possess sufficient strength withstanding the stress. Third, the coaxial configuration is constructed by layer-by-layer assembly, where the current collector is utilized as a core, followed by sequentially constructing the electrode onto the surface of
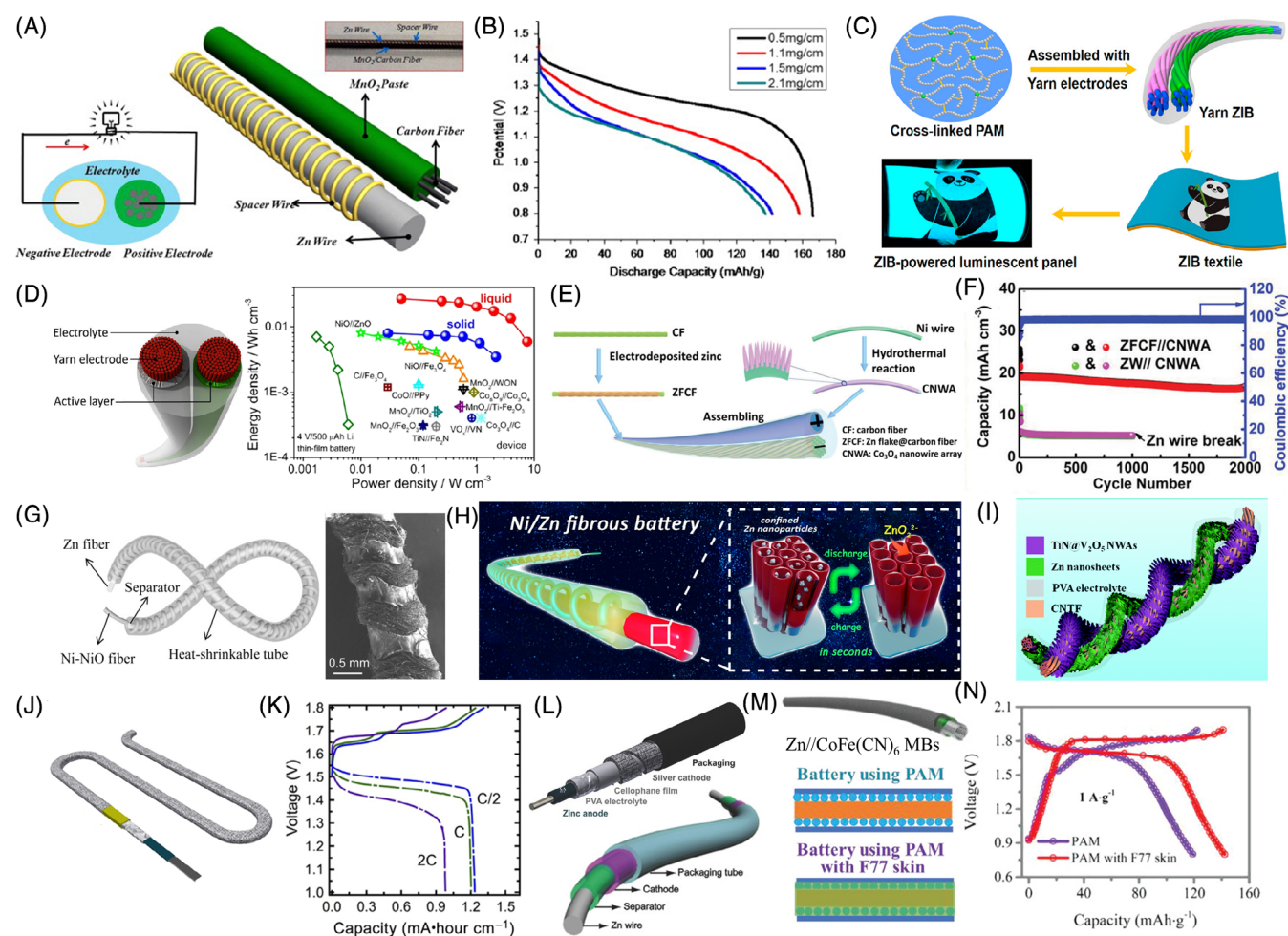


**FIGURE 3** Fiber-type ZIMBs. A, Schematic of the fiber MBs based on Zn wire and $MnO_2$/carbon fiber. The inset is the cross section of the fiber battery and the discharge process and an optical picture of Zn//$MnO_2$ battery and, B, corresponding discharging curves of the fiber battery with different $MnO_2$ loading obtained at 70 mA/g. C, Schematic of fabrication of waterproof Zn//$MnO_2$ MBs based on PAM electrolytes. D, Schematics and Ragone plot of solid-state Zn//$MnO_2$ MBs. C,D, Reproduced with permission.[44,45,50] Copyright 2017 and 2018, American Chemical Society. E, Schematic of fabrication and, F, long-term cyclability of aqueous fiber-shaped Zn//$Co_3O_4$ MBs comparing with commercially fiber Zn//$Co_3O_4$ at 1 A/cm³. G, Schematic of flexible quasi-solid-state Zn//Ni-NiO battery. H, Fabrication of Zn//Ni MBs. A,H, Reproduced with permission.[35,56] Copyright 2013 and 2018, Elsevier. I, Schematic of all-solid-state Zn//TiN@$V_2O_5$ MBs. Reproduced with permission.[42] Copyright 2019, Royal Society of Chemistry. J, Fabrication and, K, rate capability of the compliant Zn//Ag batteries. Reproduced with permission.[43] Copyright 2017, American Association for the Advancement of Science. L, Schematic of Zn//Ag MBs showing cell components and Zn//PANI MBs. M, Schematic of Zn//$CoFe(CN)_6$ MBs based on PAM electrolyte with and without F77, and, N, corresponding galvanostatic charge/discharge curves. (E-G,L-N) Reproduced with permission.[30,52,55,59,62] Copyright 2016, 2018, and 2019, Wiley-VCH. MBs, microbatteries; ZIMBs, zinc ion MBs

current collector, wrapping with gel electrolyte or separators, and then assembling the other microelectrode. And the coaxial fibers present a core-shell structure with all components of the coaxial fiber sharing the single one same axis.

### 2.1.1 | Parallel fiber ZIMBs

The first fiber ZIMBs was fabricated in a form of primary Zn-MnO$_2$ batteries with a zinc wire as anode and a dip-coated MnO$_2$/carbon fiber as cathode,[35] illustrating good flexibility without capacity loss during bending tests (Figure 3A). However, this Zn-MnO$_2$ battery was not electrochemically reversible and delivered low capacity (Figure 3B). Later, the appearance of mild neutral zinc sulfate electrolyte was helpful for the transformation of the primary Zn-MnO$_2$ batteries into a highly reversible system. For instance, Wang et al.[45] fabricated the rechargeable Zn-MnO$_2$ fiber MBs based on the MnO$_2$ electrodeposited on to the fiber-like carbon nanotubes and zinc wire in the different zinc salt electrolytes with comparably bulky anions (e.g., Zn(CF$_3$SO$_3$)$_2$, Zn(TFSI)$_2$), and small anions (ZnSO$_4$, ZnCl$_2$, etc.). Remarkably, they demonstrated the superior capacity of 290 mAh/g at 0.1 A/g, and uncoiled the effect of the molecular size of zinc salts in the electrolyte on the specific capacity and cycling stability. To develop wearable, durable, and deformable MESDs and simultaneously ameliorate low ionic conductivity, low elasticity, and poor mechanical strength of the quasi-solid-state gel poly(vinyl alcohol) (PVA) electrolyte, Li et al.[50] produced a kind of waterproof, tailorable and stretchable fiber ZIMBs (Figure 3C) with polyacrylamide (PAM) electrolyte, dip-coated MnO$_2$ cathode, and electrodeposited Zn anode. Thanks to the highly ionic conductivity of PAM electrolyte, the resulting Zn-MnO$_2$ MBs delivered high specific capacity of 302.1 mAh/g and outstanding energy density of 53.8 mWh/cm$^3$ with a high capacity retention of 98.5% after 500 cycles at 2 A/g. Moreover, splendid flexibility and strechability (up to 300% strain) of this Zn-MnO$_2$ MB was verified with a long-term cyclability (high capacity retention of 96.5%) even after 12 hours constant underwater operation.

Derived from the synergistic effects of transition metal ions, α-layered double hydroxides (α-TM(OH)$_2$, TM = transition metal, especially for bimetallic [Ni, Co] hydroxides),[79,80] Co- and Ni-based composites give rise to a new possibility for high safety, superior rate capability and energy density. Typically, Huang et al.[44] reported a wearable, conductive Zn//NiCo textile fiber MBs (Figure 3D) utilized conductive yarns of electrodeposited zinc anode and nickel cobalt hydroxide cathode, exhibiting impressive specific capacity of 5 mAh/cm$^3$, excellent rate capability up to 116 C in solid-state

electrolyte, superior power density (32.8 mW/cm$^2$ and 2.2 W/cm$^3$) and energy density (0.12 and 8 mWh/cm$^3$). In order to further improve the cyclability of ZIMBs, the fiber ZIMBs were assembled with 3D finely crafted ZnO@C-Zn anode and Co(CO$_3$)$_{0.5}$(OH)$_x$·0.11H$_2$O@CoMoO$_4$ cathode.[51] The anode was constructed by in-situ growth of the ZIF-8-derived ZnO@C nanorods as the framework onto carbon cloth and sequential deposition of Zn anode, enabling ZIMBs with admirable cyclability (82% after 1600 cycles), an impressive capacity retention of 92.5% after bending states of 100 cycles, and remarkable energy density of 4.6 mWh/cm$^3$ and power density of 0.42 W/cm$^3$. Despite of great achievements, the development of the rechargeable ZIMBs is seriously impeded by rapid growth of zinc dendrite and greatly increase of electrode irreversibility. To address these issues, combing the well-designed anode of 3D zinc flakes anchored onto the carbon fiber with N and O surficial zincophilic sites and cathode of Co$_3$O$_4$ nanowires arrayed on the Ni wire current collector, the fiber Zn//Co$_3$O$_4$ full MBs[52] (Figure 3E) were demonstrated with notable capacity retention of 90% after 2000 cycles (Figure 3F) and comparable energy density of 5.63 mWh/cm$^3$, corresponding to areal energy density of 72.5 μWh/cm$^2$.

### 2.1.2 | Twisted fiber ZIMBs

Twisted fiber MBs are favorable for knittable, weavable, and flexibly wearable MESDs, owing to the structure similar to the woven wire, which could be easily woven onto the scale-up textiles. The first demonstration of twisted Zn//Ni-NiO MBs[55] was constituted with porous Ni-NiO heterostructured nanosheets cathode without binder and zinc wire (Figure 3G) for improving the reversibility of Ni-based cathode and hindering the zinc dendrite. The interconnected Ni-NiO heterostructures were prepared with an approach of a mild hydrothermal and low-temperature calcination of Ni-based precursor, facilitating the MBs with unprecedented cyclability (100% after 10 000 cycles at 22.2 A/g), admirable energy density of 6.6 μWh/cm$^2$, and high power density of 20.2 mW/cm$^2$. Later, Li et al.[56] designed a new strategy to ameliorate the poor rate capability, short cyclability, and corrosion of anodic zinc anode, utilizing a 3D TiO$_2$ nanotube array with lithium doping supported anode (Zn@Li-RTiO$_2$) and Mn-NiO$_x$ cathode (Figure 3H). This array structure accommodated the deposited Zn as nanoparticles instead of dendrites during the charging and discharging, which was ascribed to the improved charge transport after Li doping and hydrogen-evolving property of TiO$_2$. Notably, this full MB revealed a remarkable capacity retention of 95% after 20 000 cycles, excellent volumetric energy

density of 34 mWh/cm$^3$ with power density of 17.5 W/cm$^3$. Meantime, twisted Zn//Ag MBs[53] were exploited with Ag cathode and Zn anode loaded on carbon nanotubes (loading level up to 99 wt%) by biscrolling method, devoting linear capacity in solid electrolyte of 0.276 mAh/cm. To enhance the performance of Zn//Ag$_2$O MBs, Li et al.[54] developed a quasi-solid-state Zn-Ag$_2$O MB with high electron-ion conductivity, showing high capacity of 1.05 mAh/cm$^2$, prominent energy density of 1.57 mWh/cm$^2$, remarkable power density of 14.4 mW/cm$^2$, favorable capacity retention of 79.5% after 200 cycles and high coulombic efficiency. It should be emphasized that this work made a great advance for further development of Ag-based cathode for MBs.

Owing to expensive materials of Ag and severe zinc dendrites of Zn//Ni MBs, numerous works were devoted to the development of Mn- and V-based cathode materials for fiber MBs. For instance, Wang et al.[57] unveiled the fabrication of smart Zn//MnO$_2$ MBs based on MnO$_2$ cathode coated with polypyrrole and zinc anode. The fiber MBs delivered long cyclability over 1000 cycles and a comparable capacity of 135.2 mAh/g at 1 C in quasi-solid-state electrolyte, which was ascribed to the boosting ionic conductivity and water retention properties provided by gelation-based gel. To overcome the dissolution issue of Mn-based materials, high-capacity V-based cathode materials were explored. Impressively, hierarchical core-shell structure grown on a carbon nanotube was finely designed, in which 3D highly conductive porous N-doped carbon arrays performed as core and 2D V$_2$O$_5$ nanosheets served as shell,[58] while the 3D skeleton was derived from the cobalt-based MOF nanowire arrays on the carbon nanotubes. Benefitting from the distinct structure, the all-solid-state fiber MBs extended significant volumetric specific capacity of 457.5 mAh/cm$^3$ at 0.3 A/cm$^3$ (based on the cathode), together with both high energy density of 40.8 mWh/cm$^3$ and power density of 5.6 W/cm$^3$ (based on the total volume of the device). In the meantime, another similar work in the same group for elevating the performance of V-based MBs was also carried out on 3D well-aligned TiN nanowire arrays with a core-shell heterostructure in situ grown on carbon nanotubes.[42] The as-prepared all-solid-state MBs (Figure 3I) disclosed high volumetric capacity of 405 mAh/cm$^3$ at 0.5 mA/cm$^3$, excellent cyclablity (90.6% after 3500 cycles), and outstanding energy density of 283.5 mWh/cm$^3$.

## 2.1.3 | Coaxial fiber ZIMBs

In comparison with the parallel and twisted ones, the coaxial-shaped ZIMBs display with a core-shell architecture sharing the same axis, which provided larger, closer, and more efficient active areas between cathode and anode, thus contributing to high material mass loading and superior deformation resistance. In this case, Zamarayeva et al.[43] explored the Zn//Ag MBs (Figure 3J,K) with helical springs and serpentines as current collector, which showed enhanced mechanical performance and are resilient to the deformation retaining the electrochemical performance over 17 000 bending cycles. At the same times, to extend the lifetime of Zn//Ag MBs, they reported a cathode with silver nanoparticle ink with painting onto the conductive thread and zinc anode (Figure 3L),[30] which was separated by a cellophane membrane to hinder Ag$^+$ from migrating to the zinc anode. The as-assembled Zn//Ag MBs represented favorable cyclability of almost 100% after 170 cycles, and an energy density of 53.4 Wh/L (18.35 Wh/kg).

Besides, it was reported that supercapacitor-like dual-ion mechanism of anion and cation coinserted into polymer cathode materials. For instance, Wan et al.[59] developed Zn//polyaniline (PANI) MBs (Figure 3L) with a new fashion of organic PANI cathodes grown with in situ polymerization, which performed stable capacity retention of 91.5% after 200 bending cycles. Meanwhile, Zhang et al.[60] constructed coaxial fiber MBs using MnO$_2$ as cathode protected by poly(3,4-ethylenedioxythiophene) (PEDOT) and zinc nanosheets as anode, both of which were electrodeposited onto carbon nanotube fibers, achieving prominent volumetric capacity of 12.86 mAh/cm$^3$ at 20 mA/cm$^3$, high energy density of 17.9 mWh/cm$^3$ and impressive power density of 28.1 mW/cm$^3$. To improve the operational voltage and reversibility of zinc ion insertion and extraction at high rates, the Prussian blue analogues with a 3D open framework and ample interstitial sites, were recognized as a promising cathode material for ZIMBs. As a typical example, Zhang et al.[61] demonstrated the fabrication of coaxial fiber MBs by arranging the zinc nanosheet arrays on carbon nanotube fiber as the core and zinc hexacyanoferrate (ZnHCF) on carbon nanotube as the shell. The as-fabricated MBs offered high specific capacity of 100.2 mAh/cm$^3$ and superior energy density of 195.39 mWh/cm$^3$. To explore the new electrolyte for ensuring the mechanic strength of the MBs, Ma et al.[62] invented a new-type electrolyte (Figure 3M,N) of the PAM with poly(ethylene oxide)$_{53}$-poly(propylene oxide)$_{34}$-poly(ethylene oxide) (F77), which showed a distinct sol-gel transition feature from 0°C to room temperature accompanied with the state change from aqueous to gel, contributing to the full utilization of the active material. As a result, this Zn//CoFe(CN)$_6$ MB delivered admirable long-term cyclability (93.4% after 2000 cycles).

## 2.2 | In-plane zinc ion MBs

In-plane MBs are composed of separated parallel electrodes on a single substrate, which allow fast and multidirection ions diffusion and free from separator.[7,81-86] At present, many works were contributed to optimizing the structural design of microelectrodes and decreasing the project area of the microdevices for enhancing power density and shortening the distance of ion transport. Classically, Gaikwad et al. manufactured the stretchable primary $Zn//MnO_2$ MBs[28] with polyacrylic acid (PAA)-based gel electrolyte, which offered a capacity of 3.875 mAh/cm², an open circuit potential (OCV) of 1.5 V, and surprising strechability even under strain as high as 100%. Furthermore, they powered a printed circuit directly with a printed primary $Zn//MnO_2$ battery with a voltage up to 14 V.[87] However, many stretchable MBs previously reported were fabricated with elastic

substrate, such as acrylic elastomer,[88] and fabrics.[28] To this end, Yan et al.[29] presented Zn//Ag MBs based on intrinsically stretchable Ag nanowires and zinc as electrode, which could maintain their functions even stretched up to 80% after 1000 cycles. In addition, for purpose of prolonging the cycle life, Shin et al.[39] proposed an intriguing strategy for long cycle life with the deposition of ZnO through relaxation with the help of $Bi_2O_3$.

With the development of the fiber MBs, the in-plane MBs entered their period of vigorous prosperity after the rechargeable ZIMBs appearance. Remarkably, smart flexible $Zn//LiMn_2O_4$ and $Zn//LiFePO_4$[75] MBs (Figure 4A) were constructed with the thermoreversible hydrogel as functional electrolyte (poly(ethylene oxide)-poly(propylene oxide)-poly(ethylene oxide)) by carving with knife molds. These MBs appeared with superior resistance under severe mechanical stresses and a reduced electrode-electrolyte interfacial resistance after re-wetting at low temperature
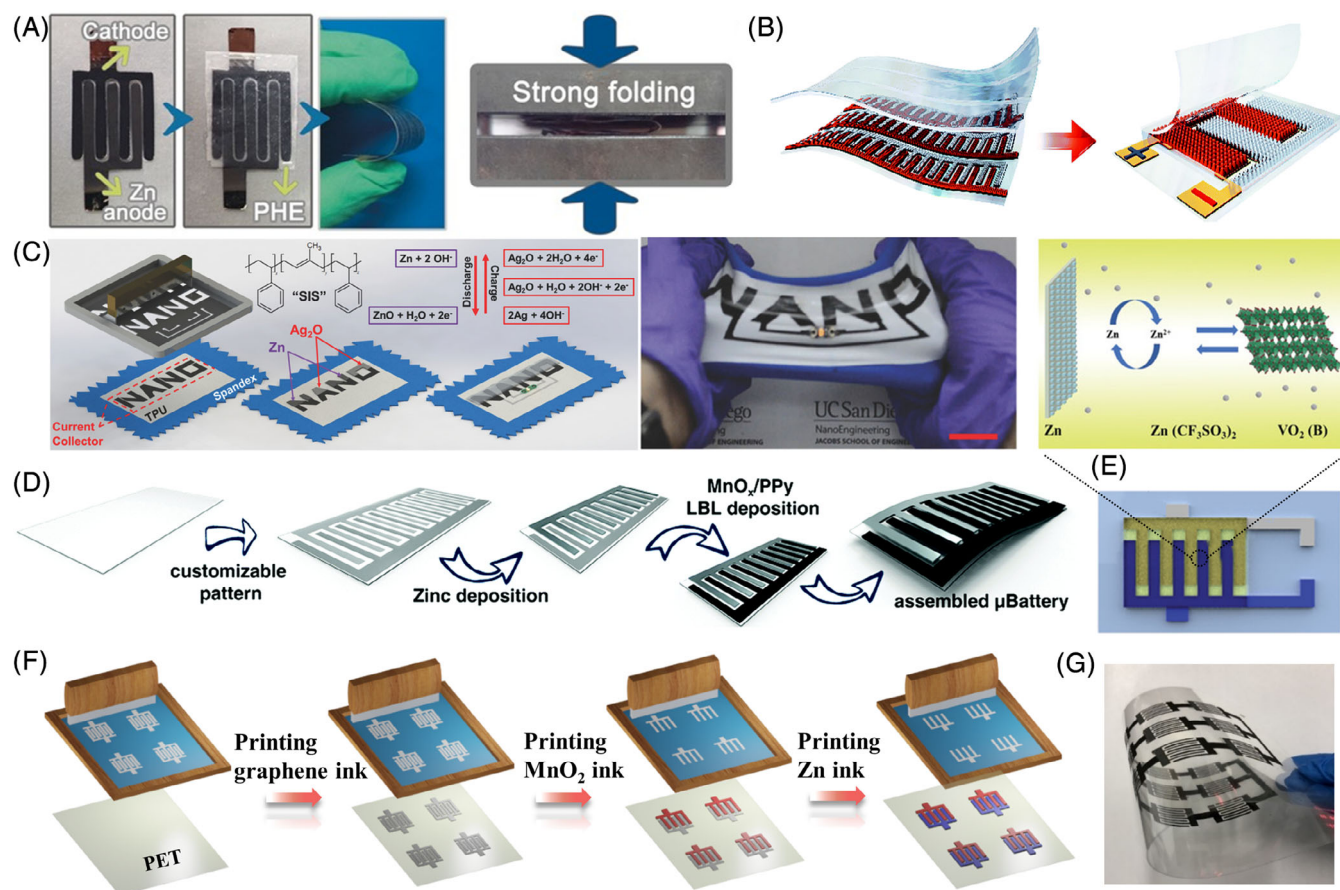


**FIGURE 4** In-plane ZIMBs. A, Optical photographs of flexible $Zn//LiMn_2O_4$ MBs in flat state and under strong folding. B, Schematic of packaged and encapsulated $Zn//MnO_2$ MBs. C, Screen-printing fabrication of $Zn//Ag_2O$ MBs on a stretchable substrate and light up a LED under the stretchable state. D, Schematic illustration of the fabrication process for $Zn//MnO_x@PPy$ MBs. B,D, Reproduced with permission.[41,77] Copyright 2018, Royal Society of Chemistry. E, The structure and working principle of $Zn//VO_2$ MBs. A,C,E, Reproduced with permission.[74,75,78] Copyright 2017 and 2019, Wiley-VCH. F, Schematic of screen-printing fabrication of printed $Zn//MnO_2$ MBs. G, Optical image of tandem printed $Zn//MnO_2$ MBs. F-G, Reproduced with permission.[11] Copyright 2019, Oxford Academic Press. LED, light-emitting diode; MBs, microbatteries; ZIMBs, zinc ion MBs

($-5°C$). It was impressive that this simple cooling process at low temperature insured the compact connection between electrode and electrolyte. Furthermore, high capacity retention was manifested with 83% and 90% after 300 cycles for $LiMn_2O_4$ and $LiFePO_4$, respectively, while the $Zn//LiMn_2O_4$ MBs delivered a reversible capacity of 71.1 mAh/g at 20 mA/g. Afterward, the environmentally benign $Zn//MnO_2$ MBs[41] assembled with 3D $MnO_2$@nickel nanocone arrays (NCAs) cathode and Zn@NCAs anode, were reported with an appealing capacity of 535 mAh/cm$^3$·at 1 C, together with superb volumetric energy density of 713 mWh/cm$^3$ and power density of 16.214 W/cm$^3$ (Figure 4B). Kumar et al.[74] printed the stretchable $Zn//Ag_2O$ MBs (Figure 4C) by incorporating polystyrene-block-polyisoprene-block-polystyrene as binder for homemade inks, leading to the assembly of all-printed $Zn//Ag_2O$ MBs with a reversible areal capacity of 2.5 mAh/cm$^2$ even after 100% stretching. Additionally, $Zn//MnO_x$@polypyrrole MBs[77] (Figure 4D) were obtained by electroplating Zn and $MnO_x$@polypyrrole onto the indium tin oxide coated with customized polyethylene terephthalate substrate, possessing a capacity of 110 μAh/cm$^2$ at 0.2 mA/cm$^2$, stable cycability after 200 cycles and high energy density of 21 mWh/cm$^3$ at 33 mW/cm$^3$. Exhilaratingly, low-cost quasi-solid-state MBs[78] were exploited with a $VO_2$ (B)-multiwalled carbon nanotubes ($VO_2$ (B)-MWCNTs) cathode, a Zn-MWCNTs anode by laser engraving and hydrogel electrolyte (Zn $(CF_3SO_3)_2$-PVA) (Figure 4E). These MBs exhibited ultra-high capacity of 314.7 μAh/cm$^2$, splendid energy density of 188.8 μWh/cm$^2$ and power density of 0.61 mW/cm$^2$. It was observed that the capacity of the MBs has no obvious decay when the temperature reached 100°C.

Taking into the large-scale, easy-process, and low-cost advancements of $Zn//MnO_2$ MBs (Figure 4F),[11] our group demonstrated high-safe $Zn//MnO_2$ MBs with superior performance, modularization and customized diversity. With the assistance of high conductive Zn ink, $MnO_2$ ink, and graphene ink as metal-free current collector, the resulting separator-free $Zn//MnO_2$ MBs were established by screen-printing technique, revealing high volumetric capacity of 19.3 mAh/cm$^3$ at 7.5 mA/cm$^3$, representative energy density of 17.3 mWh/cm$^3$ and long cyclability (83.9% after 1300 cycles). Notably, this kind of screen-printed $Zn//MnO_2$ could be built on the different substrates, for example, paper, glass, clothes, and have the great applicability for large-scale production (Figure 4G).

## 2.3 | Sandwiched zinc ion MBs

Besides the fiber and in-plane configuration, sandwiched MBs are also one of the important energy storage microdevices, which follow the traditionally stacked battery design principles, with sandwich-like geometry of cathode/separator with/or electrolyte/anode.[2] In the early stage, Ho et al.[63] exploited a direct write dispenser printing method for the construction of $Zn//MnO_2$ primary MBs with ionic liquid gel electrolyte, which was easily integrated onto the substrate. This primary $Zn//MnO_2$ MB presented a discharge capacity of 0.98 mAh/cm$^2$ and energy density of 1.2 mWh/cm$^2$. At the same time, Hiralal et al.[89] obtained the solid-state and flexible primary $Zn//MnO_2$ MBs (Figure 5A) consisted of $MnO_2$ combined with single-walled carbon nanotubes as cathode, polyethene oxide as electrolyte and zinc anode. Afterward, Gaikwad et al.[64] addressed the thickness and capacity limitations by mesh-embedded $Zn//MnO_2$ alkaline MBs architecture, with help of silver ink as current collector, PAA-based electrolyte, Zn and $MnO_2$ active ink stencil printed onto the nylon-mesh substrates. The printed MBs had a discharge capacity of 5.6 mAh/cm$^2$ at 0.5 mA. This stencil-printed way exceptionally prompted the development of the MBs with different configurations. After the electrolyte addition of $MnSO_4$ and usage of cathode protection layer for hindering the damage during charge/discharge process, the performance of rechargeable ZIMBs has been significantly enhanced. Typically, benefiting from the PEDOT buffer layer, $Zn//MnO_2$@PEDOT MBs[31] fabricated by Zeng et al. maintained more than 77.7% of initial capacity after 300 cycles, in conjunction with fantastic energy density of 33.95 mWh/cm$^3$ and power density of 8.6 kW/kg. Meanwhile, Lu et al.[40] prepared the $MnO_2$ cathode wrapped with ZnHCF (ZnHCF@$MnO_2$) by in situ coprecipitation, which combine the capacitive and intercalative properties with redox reactions. The resulting $Zn//ZnHCF@MnO_2$ MBs yielded a high average operation voltage of 1.7 V and exceptional capacity retention of 71% after 500 cycles, associated with a high-rate performance (55% capacity retention). In order to ameliorate the performance of electrolyte, Mo et al.[65] proved a smart thermoresponsive electrolyte that could be immigrated inside batteries to prevent thermal runway via smart sol-gel transition, then yielded a smart $Zn//MnO_2$ system. After that, this group developed a novel gelatin of PAM-based hierarchical electrolyte applied for the flexible quasi-solid-state ZIMBs[68] (Figure 5B,C), showing a splendid areal energy density of 6.18 mWh/cm$^2$, power density of 148.2 mW/cm$^2$, and superb cyclability (97% retention after 1000 times). This extremely safe and wearable MBs offered reliable wearability and performed well under complex conditions. Besides, they also proposed the manufacture of freeze-resistant flexible $Zn//MnO_2$ MBs[67] comprising a designed anti-freezing hydrogel electrolyte (Figure 5D,E) even at $-20°C$. This electrolyte efficiently
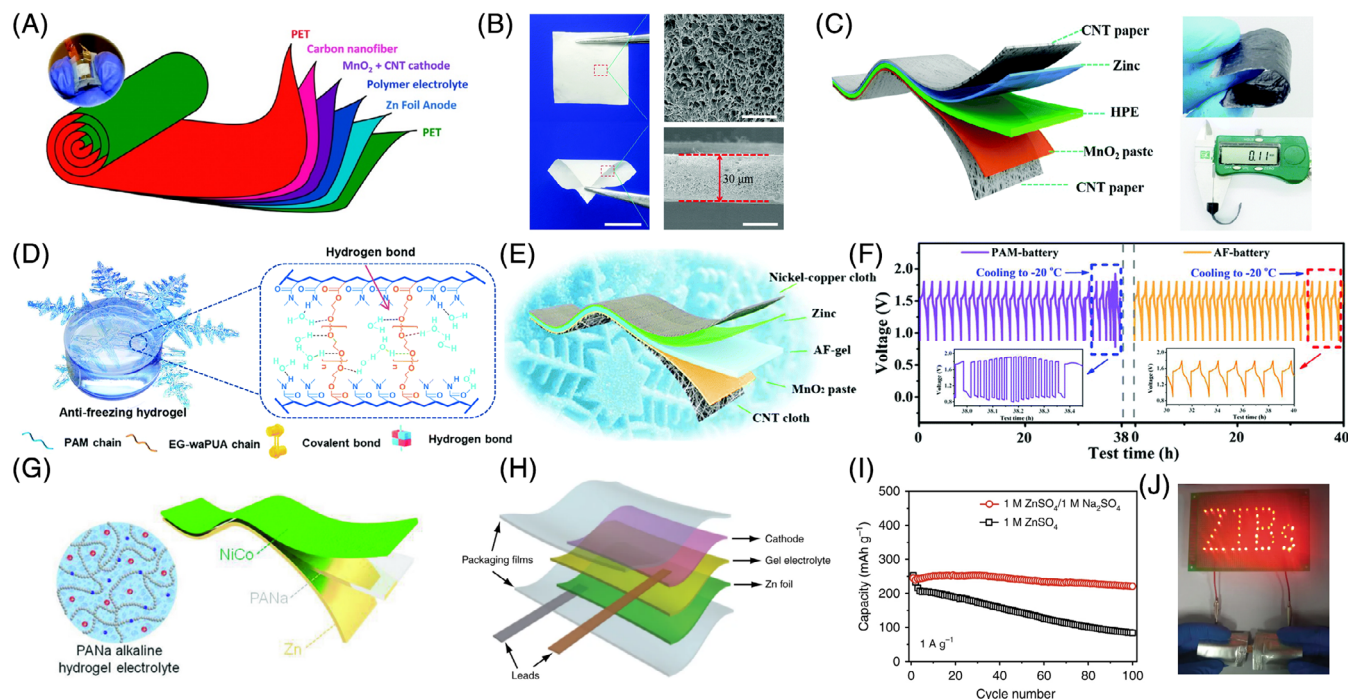
**FIGURE 5** Sandwiched ZIMBs. A, Schematic of sandwiched Zn//MnO$_2$ MBs. Reproduced with permission.[89] Copyright 2010, American Chemical Society. B, Optical image, scanning electron microscopy (SEM) image (top view) and cross-section SEM image of the hierarchical polymer electrolyte film. C, Schematic of solid-state Zn//MnO$_2$ MBs. D, Schematic illustration of the strong hydrogen bonds between EG based waterborne anionic polyurethane acrylates, water, and PAM in the antifreezing gel (AF-gel). E, Schematic of Zn//MnO$_2$ MBs based on antifreezing gel. F, Voltage profiles of Zn//MnO$_2$ MBs based on PAM and AF-gel after cooling and heating at 0.8 A/g. B-F, Reproduced with permission.[18,67,68] Copyright 2018 and 2019, Royal Society of Chemistry. G, Diagram of Zn//NiCo MBs including the PANa electrolyte, zinc anode, and NiCoOH cathode. G, Reproduced with permission.[70] Copyright 2018, Wiley-VCH. H, Diagram of Zn// NaV$_3$O$_8$·H$_2$O MBs, and, I, cycling performance at 1 A/g in ZnSO$_4$ and ZnSO$_4$/Na$_2$SO$_4$ electrolytes, and, J, optical picture of powering LED array containing 52 bulbs under bending state. H-J, Reproduced with permission.[47] Copyright 2018, Nature Publishing Group. LED, light-emitting diode; MBs, microbatteries; PAM, polyacrylamide; PANa, sodium polyacrylate; ZIMBs, zinc ion MBs

widened the working temperature range comparing with PAM electrolyte (Figure 5F) and equipped the Zn//MnO$_2$ MBs with high energy density of 32.68 mWh/cm$^3$.

With the pursuit of high capacity and high energy density, Co- and Ni-based were paid much attention owing to high theoretical capacity and large working voltage as same as the development of the fiber-type MBs. For example, Wang et al.[69] reported a Zn//Co$_3$O$_4$ MB by electrodepositing Zn anode and porous Co$_3$O$_4$ cathode on carbon fibers and Ni foam, respectively, using the electrospinning polymer of PVA-PAA as the separator. These fabricated MBs expressed high discharge voltage of 1.78 V and high energy density of 241 Wh/kg. Then, Ma et al.[18] formed the same system based on the Co$^{3+}$ rich-Co$_3$O$_4$ cathode, aided with CoSO$_4$ addition for preventing the dissolution of the cathode, which revealed unexceptional flexibility, a high voltage of 2.2 V, and notable energy density of 360.8 Wh/kg. Also, Tan et al.[90] generated a Zn//Co$_3$O$_4$ MB maintaining outstanding rate capability and energy efficiency over 70% after 200 cycles. Remarkably, Huang et al.[32] constructed a self-healing

sodium polyacrylate (PANa) hydrogel electrolyte with Fe$^{3+}$ crosslinkers that provided ionic bonding with the PANa, resulting in the superb Zn//NiCo performance. It is certified that PANa electrolyte guaranteed an order of magnitude higher cycability than the PVA electrolyte system of Zn//NiCo MBs, coupled with the zinc-free dendrites owing to the usage of quasi-solid-state electrolyte (Figure 5G).[70]

Ascribed to low cost and multivalence of vanadium, vanadium-based materials have been respected as the promising candidates for ZIMBs. Representatively, NaV$_3$O$_8$·1.5H$_2$O nanobelts synthesized by easy-processing liquid-solid stirring strategy was appeared as cathode for Zn//NaV$_3$O$_8$·H$_2$O MBs, proving stable electrochemical performance under bending state, using quasi-solid-state electrolyte (Figure 5H). Furthermore, Zn//NaV$_3$O$_8$·H$_2$O MBs showed enhanced cycling stability based on the electrolyte of ZnSO$_4$ with Na$_2$SO$_4$, demonstrating the potential of integration with light-emitting diode (LED) (Figure 5I,J).[47] Furthermore, another vanadium-based material of V$_5$O$_{12}$·6H$_2$O via electrodeposition was

**TABLE 2**  Performance comparison of the reported ZIMSCs with different configurations

| Configuration | Electrode | Voltage (V) | Electrolyte | Capacitance | Capacity retention (%)/cycle number | Power density | Energy density | Refs. |
|---|---|---|---|---|---|---|---|---|
| Interdigital | Zn//carbon nanotubes | 0.2-1.8 | $ZnSO_4$ | 83.2 mF/cm² at 1 mA/cm² | 87.4%/6000 | 8 mW/cm² | 29.6 µWh/cm² | 98 |
| Sandwich | Zn//active carbon | 0-1.8 | $Zn(CF_3SO_3)_2$ (organic) | 170 F/g at 0.1 A/g | 91%/20 000 | 1725 W/kg | 52.7 Wh/kg | 99 |
| Fiber | Zn//active carbon | 0.2-1.8 | $PVA-ZnSO_4$ | 56 mF/cm² at 0.05 mA/cm² | ~100%/10 000 | 3 mWh/cm² | 25 µWh/cm² | 100 |
| Sandwich | Zn//hollow carbon | 0.15-1.95 | $PAM-ZnSO_4$ | 86.8 mAh/g at 0.5 A/g | 98%/15 000 | 447.8 W/kg | 59.7 Wh/kg | 101 |
| Interdigital | Poly(3,3'-dihydroxy benzidine)//active carbon | 0.4-1.5 | $ZnSO_4$ | 1.1 F/cm² at 0.5 mA/cm² | 80%/3000 | 5 mW/cm² | 152 µWh/cm² | 102 |
| Sandwich | $MnO_2$//active carbon | 0-2.0 | $ZnSO_4-MnSO_4$ | 54.1 mAh/g at 0.1 A/g | 93.4%/5000 | 13 kW/kg | 34.8 Wh/kg | 103 |
| Sandwich | Zn//MXene@rGO | 0.2-1.6 | $ZnSO_4$ | 128.6 F/g at 0.4 A/g | 95%/75 000 | 279.9 Wh/kg | 34.9 Wh/kg | 104 |
| Sandwich | Zn//activated graphene | 0-1.9 | $Zn(CF_3SO_3)_2$ | 210 F/g at 0.1 A/g | 93%/80 000 | 31.4 kW/kg | 106.3 Wh/kg | 105 |
| Sandwich | Zn//N-porous carbon | 0-1.8 | $PVA-ZnSO_4$ | 148.2 mAh/g at 4.2 A/g | 73.6%/100 000 | 107.3 Wh/kg | 24.9 kW/kg | 106 |
| Interdigital | Zn//active carbon | 0.5-1.5 | $ZnSO_4$ | 1.297 F/cm² at 0.16 mA/cm² | ~100%/10 000 | 0.16 mW/cm² | 152 µWh/cm² | 107 |
| Sandwich | $Zn//RuO_2 \cdot H_2O$ | 0.4-1.6 | $Zn(CF_3SO_3)_2$ | 122 mAh/g at 0.1 A/g | 87.5%/10 000 | 16.74 kW/kg | 82 Wh/kg | 108 |

Abbreviations: PAM, polyacrylamide; PEDOT, poly (3,4-ethylenedioxythiophene); PVA, poly(vinyl alcohol); ZIMSCs, zinc ion micro-supercapacitors.

discovered with layered structure, enabling ZIMBs with high capacity of 300 mAh/g and fairish capacity retention of 96% after 50 cycles.[33] Furthermore, Zhao et al.[36] invented the flexible Zn//$V_2O_5 \cdot 1.5H_2O$ sandwiched MBs with binder-free cathode by an in situ approach, and disclosed high specific capacity of 361 mAh/g at 0.1 A/g under bending state, superb rate capability of 115 mAh/g at 2 A/g, and impressive capacity retention of 85% after 300 cycles. To sum up, there are two main approaches for improving the performance of vanadium-based materials. One is the intercalation of extra ions (such as Li,[91,92] Na,[93] Ca,[94] Zn,[95] Co,[71] Mn[96]) into the interlayer nanochannels of layered vanadium oxides. Another strategy is the insertion of crystalline water molecules as the pillar to expand the layer spacing for fast ions transfer. Besides, some materials with expanded layered structure ($MoS_2$[72]) or 3D porous framework (cyanogroup iron hexacyanoferrate[73]) were also proposed for ZIMBs with satisfactory performance.

# 3 | ZINC ION MICROSUPERCAPACITORS

Different from the ion insertion/extraction or conversion mechanism of MBs, MSCs store the energy by fast surface reactions, arising much attention due to high power density, long-term cyclability and superior rate capability, but suffer from relatively inferior energy density.[24,97] To combine the unique strengths of MBs and MSCs into one device, the hybrid ion MSCs have emerged as a highly competitive class of MESDs with high energy density and satisfactory power density, assembled by a capacitive electrode as power source and a battery-type electrode as energy source. As same as the rechargeable MBs, hybrid MSCs are usually named according to their internal shuttling ions. So far, hybrid MSCs based on monovalent metal ions have been widely investigated, while multivalent metal ion MSCs have gained limited attention, in which most studies have mainly focused on ZIMSCs because of their cost effectiveness, multivalent ions charge storage mechanism and fast ion transfer dynamics in the aqueous electrolyte. To date, the present ZIMSCs could be divided into the in-plane, sandwich, and fiber configurations. The main device configurations, electrodes, and electrochemical performance of the state-of-the-art ZIMSCs reported are listed in Table 2.

## 3.1 | In-plane microsupercapacitors

As mentioned previously, the in-plane MSCs are fabricated with cathode and anode onto one single substrate,
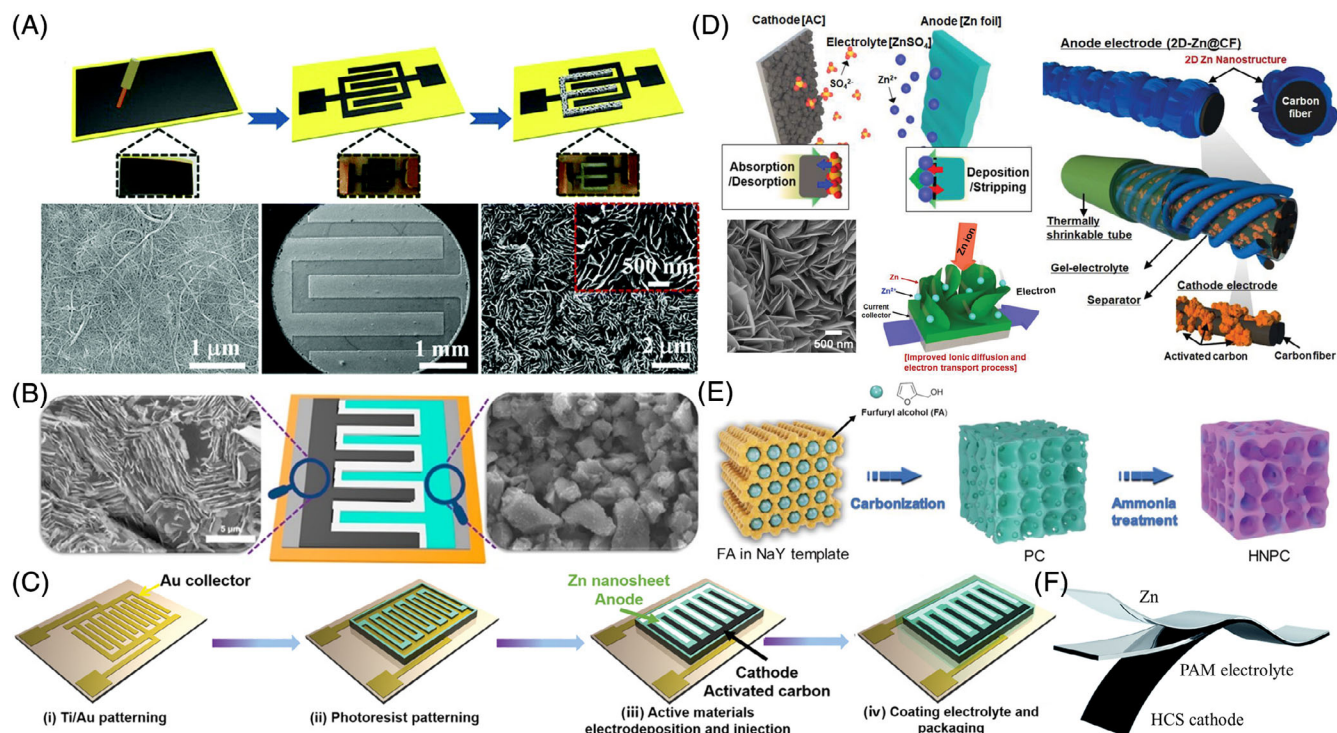
**FIGURE 6** Different configurations of ZIMSCs. A, Schematic of the preparation process of ZIMSCs, and corresponding scanning electron microscopy images of carbon nanotube, microelectrode, and anode after electrodeposition. Reproduced with permission.[98] Copyright 2018, Royal Society of Chemistry. B, Schematics of ZIMSCs based on DHB and zinc anode, corresponding SEM images. Reproduced with permission.[102] Copyright 2019, American Chemical Society. C, Schematic of the fabrication process of ZIMSCs by electrodeposition and injection. D, Schematic of flat-type ZIMSCs, 2D hierarchically nanostructured zinc anode, and structure of fiber ZIMSCs. E, Schematic of the synthesis route of N-doped hierarchically porous carbon. C-E, Reproduced with permission.[100,106,107] Copyright 2019, Wiley-VCH. F, Schematic of sandwich ZIMSCs. Reproduced with permission.[101] Copyright 2019, Royal Society of Chemistry. DHB, poly(3,3′-dihydroxybenzidine); ZIMSCs, zinc ion microsupercapacitors

separated by an empty physical spacing with widths of several or hundreds of micrometers.[109] Initially, Sun et al.[98] constructed the first ZIMSC with battery-type zinc anode and capacitor-type carbon nanotube cathode, as shown in Figure 6A. The interdigital microelectrodes of ZIMSC were fabricated by laser engraving of carbon nanotube paper pasted on the polyimide tape, following by electroplating the zinc anode on one side of the interdigital microelectrodes. In the meantime, they offered a novel strategy of recoverable zinc anode by in situ electroplating the anode without destruction of microelectrodes, which sufficiently alleviated the issue of irreversible consumption of zinc anode and capacity fading during the charge/discharge process. The as-prepared ZMSCs displayed excellent areal capacitance of 83.2 mF/cm$^2$ at 1 mA/cm$^2$, remarkable energy density of 29.6 μWh/cm$^2$ and power density of 8 mW/cm$^2$, as well as high capacity retention of 87.4% after 6000 cycles. However, carbon nanotube as cathode supplied with a low capacitance of the ZIMSCs. To address this stumbling issue, an effective strategy was to apply

the materials with high pseudocapacitance into the cathode. For instance, Wang et al.[102] devised an innovative cathode of a pseudocapacitance polymer (poly(3,3′-dihydroxybenzidine) [DHB]) electrodeposited onto the surfaces of porous active carbon and zinc anode by electrodeposition (Figure 6B). Assisted with the pseudocapacitance polymer, the resulting ZIMSCs exhibited ultrahigh areal capacitance of 1.1 F/cm$^2$ and maximum areal energy density of 152 μWh/cm$^2$, in conjunction with high capacity retention of 80% after 3000 cycles. For the same purpose, Zhang et al.[107] built the in-plane ZIMSCs (Figure 6C), composed of battery-type electrodeposited zinc nanosheet anode and the capacitor-type active carbon cathode with fast ion adsorption/desorption mechanism, fabricated by the refined process of photolithography, electrodeposition, and injection. As a consequence, the fabricated ZIMSCs revealed landmark areal capacitance of 1297 mF/cm$^2$ at 0.16 mA/cm$^2$, outstanding areal energy density of 115.4 μWh/cm$^2$ at 0.16 mW/cm$^2$ without obvious capacity decay after 10 000 cycles.

## 3.2 | Other type microsupercapacitors

As known, conventional ZIMSCs[99,103,105,108] with sandwich configuration store the energy through both the Faradaic redox reactions on the surface of anode ($Zn/Zn^{2+}$) and the formation of electric double layers with electrolyte ions on the cathode. To improve the capability of storing energy, 2D hierarchically nanostructured zinc metal (2D-Zn) was electrodeposited onto the surface of the carbon fiber by voltage-tailored electrodeposition. As illustrated in Figure 6D, the fiber-type ZIMSCs[100,110] were successfully fabricated with 2D-Zn structures on carbon fibers as anode and active carbon casted onto the carbon fibers as cathode, separated by cellulose papers. This well-designed nanostructure supplied the fiber-type ZIMSCs with improved ions diffusion and electron transport, contributing to high areal capacitance of 56 mF/cm$^2$ at 0.05 mA/cm$^2$, high energy density of 25 μWh/cm$^2$ and power density of 50 μW/cm$^2$, as well as high capacity retention of nearly 100% after 10 000 cycles. However, impeded by the limited specific surface area of the corresponding carbonic cathodes and charge storage capacity via adsorption/desorption of zinc ions in the Helmholtz layer even in the 2D hierarchically structure, the energy density is far from satisfactory especially at high rates. To overcome this issue, a robust sandwich ZIMSC consisted with a cathode of self-designed N-doped hierarchically porous carbon[106] and zinc anode. The poriferous architectures with large surface area and the incoming N dopants favoring the adsorption/desorption of zinc ions during charge/discharge, contributed to the exceptional capacity of 148.2 mAh/g at 4.2 A/g, excellent capacity retention of 88.3% after 10 000 cycles, high power density of 27.6 kW/kg and energy density of 91.8 Wh/kg. As another example, Chen et al[101] introduced a flexible sandwich ZIMSC (Figure 6F) composed of the copolymer derived hollow carbon spheres as cathode, PAM hydrogel as electrolyte and zinc anode deposition on carbon cloth. Due to high surface area and hollow structure of the cathode, the ZIMSCs unveiled robust capacity of 86.8 mAh/g, exceptional energy density of 59.7 Wh/kg, large power density of 447.8 W/kg, combining with admirable capacity retention of 98% after 15 000 cycles.

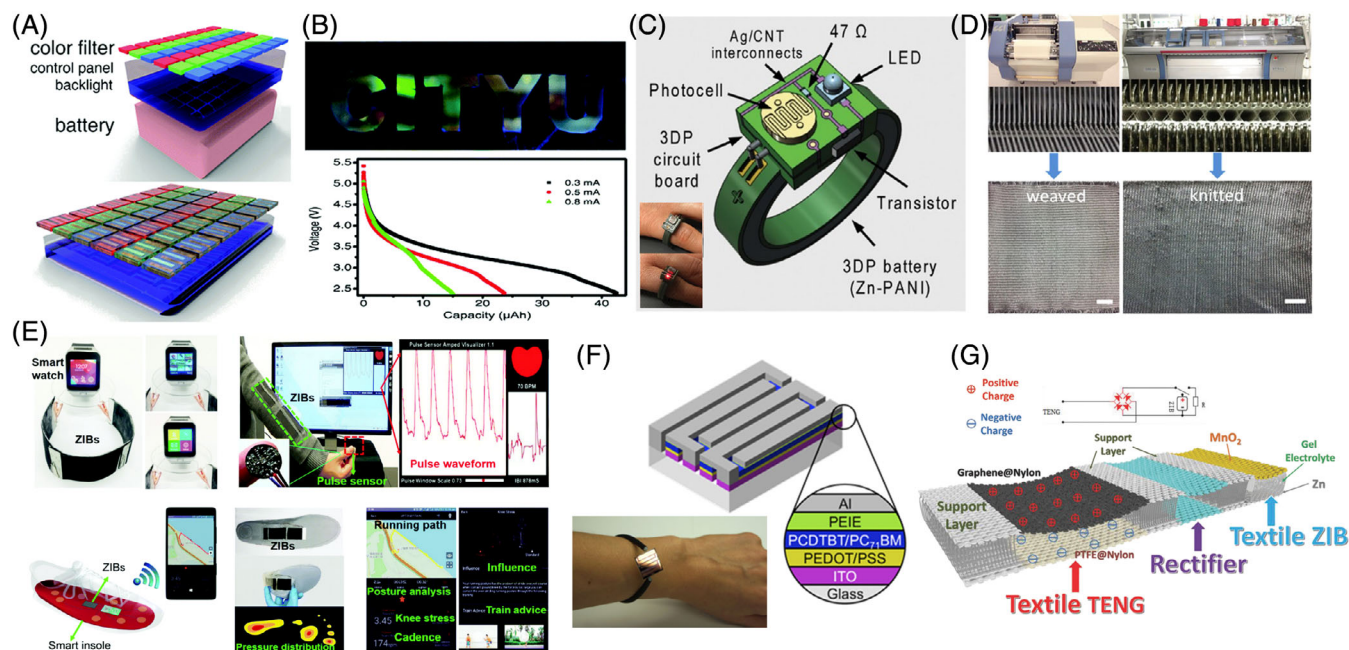## 4 | FLEXIBLE AND SMART INTEGRATED SYSTEMS

Although the MESDs have scored tremendous achievements so far, but there is still a long way for realizing practical applications of individual MESDs. At present, most electrical devices are supplied by external and unportable power sources, with bulky volume and heavy mass, which cannot meet the booming demand of the portable and implantable self-powered miniaturized electronics. Till now, the state-of-the-art MESDs could provide with areal energy density of 10−2 to 10 mWh/cm$^2$ from MBs and power density of 10 to 103 mW/cm$^2$ from MSCs. However, to realize high energy from microwatts to watts for powering the microelectronics,[5] the self-integration modularization of parallel and serial connection in a well-designed fashion is acknowledged as a more reliable strategy.[7,8,81] Besides, the MESDs could be integrated with microsized energy harvesters (eg, solar cells, nanogenerators) to provide high peak power, reasonable energy density for consumer microelectronics. Despite of the advances of innovative MESDs and self-powered systems demonstrated, the development of smart integrated systems are still in their infancy.

Miniaturized electronics could be readily integrated with different MESDs for the prosperous targeting applications. Typically, a battery-in-screen configuration could be realized by replacing the color filter in a liquid crystal display screen with the ZIMBs (Figure 7A).[77] The miniaturized ZIMBs integrated with the color filter in one layer was wired on the screen to supply power, which could be directly powered by ZIMBs (Figure 7B). For wearable and flexible MESDs, customized battery with specified capacity and voltage was crucial for certain applications. As exemplified, aqueous Zn//PANI ZIMBs[111] were established by packaging with vertically stacked and interconnected electrodes. And an integrated photosensor was constructed, constituted with a ring-shaped battery, a photocell, a resistor (47 Ω), a transistor and a LED (Figure 7C). A ring-shaped integrated microdevice was successfully formed based on the in-series Zn//PANI MBs, possessing a capability of lighting up a red LED when the photocell detected a certain of darkness.

Recently, wearable systems have gained increasing attention, which required an appropriate and high-safety power source as power supply in various applications of smart watch, health monitor and various sensors. Especially, the strechability of zinc ion MESDs is important when integrated with wearable electronics,[113-115] composed of an elastic gel membrane, stretchable electrolyte and electrode with superior mechanical performance. And an all-stretchable-component energy storage device has been successfully established with robust mechanical deformability.[113] For instance, a smart watch integrated with ample electronic components including a processor, display and sensors, thus demanding of a powerful energy supplier. For example, the as-fabricated Zn//MnO$_2$ MBs[116] could stubbornly survive after placing it onto the shoes and walking on it for 2 days, even when it

**FIGURE 7** Flexible and smart integration systems based on zinc ion MESDs. A, Schematic of the principle of ZIMBs array as a color filter, under ultraviolet light illumination. B, Simulation of the full color display with RGB pixels and galvanostatic discharge curves of ZIMBs array measured at 0.3, 0.5, and 0.8 mA. C Schematic of integration of wearable photo sensor with ring-shape Zn//PANI MBs and a 3D-printed circuit board and corresponding photographs in bright and dark conditions. D, Optical photographs of industrial weavability and knittability of Zn//NiCo MBs. C,D, Reproduced with permission.[44,111] Copyright 2017 and 2018, American Chemical Society. E, Schematic of integrated ZIMBs with other smart systems. A,B,E) Reproduced with permission.[68,77] Copyright 2018 and 2019, Royal Society of Chemistry. F, Structure of organic photovoltaic module and its integration with Zn//Ag MBs in one bracelet. Reproduced with permission.[43] Copyright 2017, American Association for the Advancement of Science. G, Fabrication protocol and schematic of integrating ZIMBs with the nanogenerator. Reproduced with permission.[112] Copyright 2018, Wiley-VCH. MBs, microbatteries; MESDs, microelectrochemical energy storage devices; ZIMBs, zinc ion MBs

was fixed onto the wheel of the car for 20 minutes exposure on the road. Owing to the appearance of industrial weavability and knittability of Zn//NiCo MBs (Figure 7D), the integration with other smart systems easily realized on the fabrics. For example, in order to better integrate the MESDs into the clothes with the sensor, smart microdevices and other wearable microelectronics, the knittable fabrics were applied for constructing Zn//Co$_3$O$_4$ MBs[66,117] with other smart electronics, including the wearable sensor, wearable electronics, and smart glass. As another example, Li et al.[68] invented a flexible energy supplier for smart watch. In this case, three Zn//MnO$_2$ MBs were connected in series and attached the smart watch to guarantee the well-operation, and further all functions were realized without accidents. Meanwhile, the health monitor system integrated with four serially connected Zn//MnO$_2$ MBs into T-shirt was also successfully constructed to collect pulse wave data and heart rate, which could easily imply the human physiological state under flat and bending states. It was interesting that the smart insoles were applied to build a high-resolution in-shoe measurement system which could offer real-time information while running, walking and other human

activities, indicative of great potential in rehabilitation, sports and medical diagnostics. These smart insoles consisting of various smart sensors could collect and transfer real-time information via a bluetooth-connected mobile phone, exhibiting a strong resistance from external strain when walking, running, and jumping on the top of the smart insoles (Figure 7E). Impressively, it could list a detailed report even running after 2.1 km with the assistance of Zn//MnO$_2$ MBs, involving knee stress, gait, compressive evaluation and contact flight ratio.

To efficiently convert the renewable energy (such as solar, friction, mechanical, and thermal energy) into electricity and timely supply power for smart microdevices, an effective strategy is to develop the integrated systems consisting of energy harvester (eg, solar cells, nanogenerators), energy storage system (eg, MBs, MSCs), and energy conversion devices. Typically, utilizing solar energy to generate the power and supply electrical energy for MBs and MSCs is a reliable way to establish energy autonomous system. Therefore, an integrated power source in a bracelet was designed based on organic photovoltaic module (Figure 7F) and fiber Zn// Ag battery.[43] Furthermore, triboelectric nanogenerators

(TENGs) and Zn//MnO$_2$ MBs[112] with the 3D spacer fabrics were successfully integrated with the help of rectifier (Figure 7G), which had a three-layer configuration separated by mediate support layer with up and down layer, serving as the flexible substrate, in which the space could be filled with gel electrolytes. It was verified that the energy storage efficiency of the electrical energy provided by TENGs was up to 39.8%. For other energy utilization, a wind-generator and a flexible Zn//Ag$_2$O fiber MB[54] were combined to enable gathering and storing wind energy, and the generator have great capability for converting the wind energy into electricity. Afterwards, a smart integrated system of the fully solar-powered coaxial stretchable sensing fiber system[60] was fabricated, involving solar cells for energy harvest, aqueous Zn//MnO$_2$ battery for energy storage, and a strain sensor for energy conversion. More specifically, the solar cells supplied the energy by converting the solar energy into electricity and fiber Zn//MnO$_2$ MBs stored as chemical energy, existed as a constant and continuous energy supplier for strain sensor, which worked synergistically to ensure the stable operation of the solar-powered coaxial stretchable sensing fiber systems.

# 5 | SUMMARY AND PERSPECTIVES

In summary, we review the state-of-the-art advances of zinc ion MESDs in both MBs and microsupercapacitors for the smart integrated systems. Briefly, the importance and current status of zinc ion MESDs with the fiber, in-plane, and sandwiched configurations are described in details, with an emphasis on the construction of ZIMBs and ZIMSCs with high-performance and multifunctional form factors and fundamental understanding of their energy storage mechanism. Moreover, the progresses of zinc ion MESDs for flexible and smart integrated systems are presented to highlight environmental adaptability, scalability, and applicability.

With the ever-increasing interest in safe, flexible, miniature, and wearable electronics, enormous efforts have been devoted to zinc-based MESDs from ZIMBs to ZIMSCs, as summarized above. It is worth noting that, only if addressing the challenging issues of safety, low cost, wide working temperature range, large voltage operation, high energy/power density, long-term cycability, and compatible integration, their practical applications of zinc-based MESDs in the future will be realized. But in our opinion, the following challenges and technical problems should be seriously considered to accelerate the development of zinc-based MESDs.

## 5.1 | Screening of high-capacity cathodes and design of extremely stable anodes

It is well accepted that the capacity of cathode and anode materials is one of the key factors for determining the performance of both MBs and MSCs. In general, zinc anode usually works both as current collectors and active material at the same time, but zinc metal is directly appeared without decoration, leading to the irreversible side reactions, H$_2$ revolution, corrosion, zinc dendrite growth, and passivation that definitely decrease the energy density to some extent. To mitigate this issue, the promising strategies of anode protection include the reasonable construction of zinc anode with hierarchical architecture or zinc hybrids,[100] uniform coating of inert layer on zinc anode,[51,118] synthesis of appropriate crystal zinc structure,[98] and introduction of effective additives into electrolytes.[39] Specifically, hierarchical architectures, such as 3D skeleton matrix zinc anode, supply high surface area with enriched active sites for ions accommodation, enhanced electrode permeability, producing uniform electric field streamlines and minimizing Zn nuclei size effectively. In addition, surface coating and interface modification have been demonstrated as effective strategies to address the issues of zinc anode,[119] such as porous protective layer on the Zn surface,[120] and introduction of artificial solid electrolyte interface.

On the other hand, since zinc anode possesses high theoretical capacity of 825 mAh/g, the present capacity of the report cathodes cannot well match with this high capacity of anode. Currently, the Mn-, V-, and Prussian blue-based materials have been demonstrated to greatly enhance the performance of zinc storage. Undoubtably, high-performance cathode materials containing multiple-electron redox reaction, ample active sites and high conductivity (such as Co[III] rich-Co$_3$O$_4$,[18] cyanogroup iron hexacyanoferrate,[73] oxygen-deficient MnO$_2$,[121] conductive metal-organic framework[122]), especially intercalation-pseudocapacitive layered materials, are highly demanded, and their increased zinc ion storage capability would be realized by combining the defect/vacancy engineering (eg, heteroatom doping, oxygen vacancies), modification of surface/interface, construction of highly conductive heterostructures, and enlargement of the interlayer spacing in 2D-layered materials.

## 5.2 | All-climate and solid-state electrolytes

As mentioned above, the electrolyte for zinc ion MESDs contains neutral (or mild acid) and some alkaline aqueous solution. Compared to neutral electrolyte, the

alkaline electrolyte contributes to the irreversible capacity, severe zinc dendrites, and passivation.[123] Generally, the most used $ZnSO_4$ solution suffers from the intrinsically limited solubility and low zinc stripping/plating coulombic efficiency, while the $Zn(CF_3SO_3)_2$ presents a smaller polarization and higher coulombic efficiency, since the bulky $CF_3SO_3^-$ anion decreases the number of the water molecules surrounding the $Zn^{2+}$ and reduce the solvation effect.[124] Besides, high concentrated aqueous electrolyte, such as $Zn(TFSI)_2 + LiTFSI$,[125] could exhibit dendrite-free stripping/plating of zinc with nearly 100% coulombic efficiency due to the formation of close ion pairs $(Zn-TFSI)^+$ suppressing the formation of $(Zn-[H_2O]_6)^{2+}$ and $H_2$ evolution. Additionally, preadded $Mn^{2+}$ additives can provide an appropriate equilibrium between $Mn^{2+}$ dissolution and the reoxidation of $Mn^{2+}$ in the electrolyte.[126]

To satisfy environmental adaptability and increase the energy density, it is urgent to explore the all-climate, high-safe, and high-voltage zinc ion MESDs. However, the aqueous electrolyte will be frozen below 0°C or boiled over 100°C at one bar pressure, and suffers from narrow working potential windows, which is not suitable for high-energy-density zinc ion MESDs working at the wide temperature range. The aqueous electrolyte might cause the serious leakage issues when the device is operated in highly complex states such as scrolling, pressing, twisting, stretching, and other destroying actions. One feasible solution for this issue is devoted to the development of new quasi-solid-state electrolytes (eg, ionogel, PAM, PVA, and PANa-based electrolytes) and even all-solid-state electrolytes (eg, metal oxide inorganic electrolyte), owing to their advantages of outstanding electrochemical stability under low/high temperature, wide working voltage and easy processing of encapsulation. But there is still a long way to realize the practical utilization since the insufficient ionic conductivity, unsatisfactory mechanical stability and lack of fundamental understanding of the interfacial chemistry between electrode and electrolyte. Besides, the "water-in-salt" electrolytes,[125] characteristic of retarded oxygen and hydrogen evolution by the excessively concentrated salt solution, is a highly competitive choice to widen the working voltage window of the aqueous electrolyte on the promise of high safety. In the "water-in-salt" electrolyte, the zinc ion hydration could be limited by the high concentration of $Li^+$, $Na^+$, and $Al^{3+}$,[127] which could impede the side reaction of hydrogen evolution reaction. Furthermore, the effective additives,[118,127] such as special polymers, organic molecules and metal ions of $Bi^{3+}$ and $Pd^{2+}$, could be considered as one of the key knacks for the zinc dendrites suppression in the improvement of long-term cyclability, high energy density and high safety of zinc-based MESDs.

## 5.3 | High energy density and power density

For high energy density, there are two main factors of specific capacity and cell voltage that are responsible for energy density. Therefore, there are three ways for improving the energy density by (a) increasing the potential of the cathode, (b) increasing the number of the electrons involved in the redox reactions for improving specific capacity, and (c) decreasing the molecular weight of electrode materials.[115,128] For high power density, besides improving the voltage, another approach is focused on the enhancement of the reaction kinetics, which could reduce the over potentials and hinder the fast voltage decay. In this case, the decisive part for high energy/power density is the choice and design of electrode materials. Furthermore, the configuration of high energy density devices with a proper electrode material could be diverse. In particular, the in-plane configuration could be more likely to meet the demands of high energy/power density, since they can provide a 3D ion diffusion transport mechanism[129] with increased loading mass and free of the separator, and possess the capability of miniaturization with a customized shape.

So far, several effective strategies for high energy density and power density have been developed.[130] The first efficient strategy is the optimization of electrode materials.[18,34] Large capacity and high voltage cathode materials conjunct with large capacity and low potential anode materials could contribute to the increase in energy density. Those active materials should provide a fast electron-ion transfer path and increase specific surface area to supply more active sites. The second one is the structural engineering of electrodes with increased loading mass and decreased binders and conductive additives.[131] Unique electrode design is of great importance for realizing high energy density without sacrificing the flexibility, such as self-supporting electrodes, honeycomb-patterned current collector, spine-like electrode with the hard component for energy storage and the soft component for flexibility provider. The third strategy is to develop high voltage electrolytes.[127] Especially, all-solid-state electrolytes with high voltage, mechanical robustness, high ionic conductivity, and small electrode/electrolyte interface resistance are promising for next-generation zinc-based MESDs.

## 5.4 | Innovative device configuration

In view of the device geometry of zinc ion MESDs, there are three main types of fiber, in-plane, and sandwiched configurations. The major purpose of developing each

configuration is to satisfy the different application scenarios, for example, fiber MESDs for wearable electronics, in-plane MESDs for ultrathin-customized and miniature electronics, and sandwich MESDs for flexible electronics. Moreover, novel configurations, such as nanowire microdevices for in situ probe, 3D-interconnected configuration for promoting the ion transport, are supposed to be developed for further understanding the fundamental mechanism of the flexible microdevices and improving the whole capacity. With the rapid development of Internet of Thing, wearable, and miniature electronics, the key requirement is to construct high-performance zinc-based MESDs with various functional properties on a flexible, stretchable and customized substrate. Another important factor is the development of three-dimensional electron-ion conductive easy-processing configuration, which is decided by three counterparts, including the electron/ion conductivity of microelectrode, the ion conductivity of electrolyte and the interfacial resistance between electrode and electrolyte. In particular, well-designed configuration should be proposed for supplying high areal and volumetric energy density of zinc-based MESDs based on the sufficient utilization in a customized project area, which will have a significant impact on the dynamics of ions and electronics. What's more, the innovative design will be helpful for the construction of highly safe zinc-based MESDs for smart integration systems on one single substrate, which is one of the greatest challenges in the road of realizing industrial applications.

## 5.5 | Developing scalable fabrication and encapsulation techniques

The present manufacturing techniques, such as doctor blading, knife graving, electrodeposition, photolithography are still far from satisfactory for the practical applications. To overcome this issue, cost-effective, easy-processing, and scalable fabrication techniques must be explored, in particular, printing technologies, such as inkjet printing, screen printing, 3D printing. In order to use these techniques, high-quality well-defined inks should be controllably prepared to construct the stable and highly conductive electrode for MESDs, printed onto the different substrates. Particular emphasis is given to the flexible MESDs which require highly stable contact of the formed electrodes with the printed substrate and efficiently withstand the severe deformation. In addition, it should be stated that the unconventional encapsulation of MESDs, sealed by the encapsulated materials such as polydimethylsiloxane, polyurethane or other elastic polymers, presently is still in the early development stage, which should be paid much attention to substantially

prevent the leakage of liquid electrolyte and thus guarantee high performance and stability of zinc-based MESDs.

## 5.6 | Fabrication of multifunctional highly integrated systems with satisfactory mechanical stability

In order to realize the multifunctional and integrable systems, numerous features are demanded such as self-healing, photo sensing, and pressure sensing. The high safety of environmentally friendly zinc-based MESDs makes these self-powered integrated systems promise for many emerging applications such as biomimetic, healthcare, artificial intelligence, modern optoelectronics, sensing microelectronics, and other energy-related devices. For instance, the fiber MESDs have a great potential in the wearable devices due to its knittable nature and similarity with fabrics. More importantly, the energy efficiency is supposed to evaluate the overall performance of the integrated systems, which could be likely improved by selecting the proper matched electronics, including energy harvester (eg, solar cells, nanogenerators), energy storage system (eg, ZIMBs, ZIMSCs) and energy conversion devices (eg, sensor), for the integration of MESDs.

However, mechanical stability is one of the most important performance when evaluating the devices property. To realize good mechanical stability, there are several important strategies developed.[132] First, the electrode and current collectors should possess good mechanical stability under severe deformation. The current collectors should be chemically compatible with the active layers and have good adhesion to prevent delamination during flexing and calendaring. Effective strategies have been realized without metal current collectors or with thin evaporated metals.[85] Second, the flexible and/or stretchable substrate is supposed to supply good mechanical stability. Also, the packaging materials should be flexible, sealable, resistant to corrosion and chemically resistant to aqueous and organic solvents/chemical products in the battery.[28] Third, the electrode microstructure could be designed to disperse the deformation pressure, such as spine-like electrode,[128] bamboo-slip-like electrode, in which the hard component could work as energy storage and the soft component could work as flexibility provider. The last but not least, all-solid-state electrolyte[133] could contribute to high mechanical stability, and then avoid the leakage of aqueous electrolyte under the severe deformation.

In brief, great significance is put on the exploration and optimization of high performance cathode, anode and electrolyte, combined with the novel configuration and

further understanding of the mechanism. Importantly, the synergistic optimization of the whole devices including encapsulation and energy conversion efficiency should be overally considered. Therefore, zinc-based MESDs are a very important class of high-safety, cost-effective micro-scale power source, and holds great promise for the future wearable and miniaturized smart integrated systems.

## CONFLICT OF INTEREST

The authors declare no potential conflict of interest.

## ORCID

*Zhong-Shuai Wu* https://orcid.org/0000-0003-1851-4803

## REFERENCES

1. Li Y, Fu J, Zhong C, et al. Recent advances in flexible zinc-based rechargeable batteries. *Adv Energy Mater*. 2019;9:1802605.
2. Yu P, Zeng YX, Zhang HZ, Yu MH, Tong YX, Lu X. Flexible Zn-ion batteries: recent progresses and challenges. *Small*. 2019;15:27.
3. Zheng S, Shi X, Das P, Wu ZS, Bao X. The road towards planar microbatteries and micro-supercapacitors: from 2D to 3D device geometries. *Adv Mater*. 2019;31:e1900583.
4. Peng HJ, Huang JQ, Zhang Q. A review of flexible lithium-sulfur and analogous alkali metal-chalcogen rechargeable batteries. *Chem Soc Rev*. 2017;46:5237-5288.
5. Zhang P, Wang F, Yu M, Zhuang X, Feng X. Two-dimensional materials for miniaturized energy storage devices: from individual devices to smart integrated systems. *Chem Soc Rev*. 2018;47:7426-7451.
6. Wang Y, Liu B, Li Q, et al. Lithium and lithium ion batteries for applications in microelectronic devices: a review. *J Power Sources*. 2015;286:330-345.
7. Shi X, Pei S, Zhou F, et al. Ultrahigh-voltage integrated micro-supercapacitors with designable shapes and superior flexibility. *Energ Environ Sci*. 2019;12:1534-1541.

8. Zheng S, Ma J, Wu Z-S, et al. All-solid-state flexible planar lithium ion micro-capacitors. *Energ Environ Sci*. 2018;11:2001-2009.
9. Manthiram A. An outlook on lithium ion battery technology. *ACS Cent Sci*. 2017;3:1063-1069.
10. Gwon H, Hong J, Kim H, Seo D-H, Jeon S, Kang K. Recent progress on flexible lithium rechargeable batteries. *Energ Environ Sci*. 2014;7:538-551.
11. Wang X, Zheng S, Zhou F, et al. Scalable fabrication of printed $Zn//MnO_2$ planar micro-batteries with high volumetric energy density and exceptional safety. *Natl Sci Rev*. 2020;7:64-72.
12. Canepa P, Sai Gautam G, Hannah DC, et al. Odyssey of multivalent cathode materials: open questions and future challenges. *Chem Rev*. 2017;117:4287-4341.
13. Ponrouch A, Frontera C, Barde F, Palacin MR. Towards a calcium-based rechargeable battery. *Nat Mater*. 2016;15:169-172.
14. Fang GZ, Zhou J, Pan AQ, Liang SQ. Recent advances in aqueous zinc-ion batteries. *ACS Energy Lett*. 2018;3:2480-2501.
15. Kaveevivitchai W, Manthiram A. High-capacity zinc-ion storage in an open-tunnel oxide for aqueous and nonaqueous Zn-ion batteries. *J Mater Chem A*. 2016;4:18737-18741.
16. Konarov A, Voronina N, Jo JH, Bakenov Z, Sun YK, Myung ST. Present and future perspective on electrode materials for rechargeable zinc-ion batteries. *ACS Energy Lett*. 2018;3:2620-2640.
17. Ming J, Guo J, Xia C, Wang W, Alshareef HN. Zinc-ion batteries: materials, mechanisms, and applications. *Mat Sci Eng R*. 2019;135:58-84.
18. Ma L, Chen S, Li H, et al. Initiating a mild aqueous electrolyte $Co_3O_4$/Zn battery with 2.2 V-high voltage and 5000-cycle lifespan by a Co(III) rich-electrode. *Energ Environ Sci*. 2018;11:2521-2530.
19. Zhao Q, Huang W, Luo Z, et al. High-capacity aqueous zinc batteries using sustainable quinone electrodes. *Sci Adv*. 2018;4:eaao1761.
20. Yi F, Ren H, Shan J, Sun X, Wei D, Liu Z. Wearable energy sources based on 2D materials. *Chem Soc Rev*. 2018;47:3152-3188.
21. Lobo DE, Banerjee PC, Easton CD, Majumder M. Miniaturized supercapacitors: focused ion beam reduced graphene oxide supercapacitors with enhanced performance metrics. *Adv Energy Mater*. 2015;5:1500665.
22. Ferris A, Reig B, Eddarir A, et al. Atypical properties of fib-patterned ruox nanosupercapacitors. *ACS Energy Lett*. 2017;2:1734-1739.
23. Mo FN, Liang GJ, Huang ZD, Li HF, Wang DH, Zhi CY. An overview of fiber-shaped batteries with a focus on multifunctionality, scalability, and technical difficulties. *Adv Mater*. 2020;32:33.
24. Qi D, Liu Y, Liu Z, Zhang L, Chen X. Design of architectures and materials in in-plane micro-supercapacitors: current status and future challenges. *Adv Mater*. 2017;29:1602802.
25. Meng J, Guo H, Niu C, et al. Advances in structure and property optimizations of battery electrode materials. *Joule*. 2017;1:522-547.
26. Pan H, Shao Y, Yan P, et al. Reversible aqueous zinc/manganese oxide energy storage from conversion reactions. *Nat Energy*. 2016;1:16039.

27. Kaltenbrunner M, Kettlgruber G, Siket C, Schwodiauer R, Bauer S. Arrays of ultracompliant electrochemical dry gel cells for stretchable electronics. *Adv Mater*. 2010;22:2065-2067.

28. Gaikwad AM, Zamarayeva AM, Rousseau J, Chu HW, Derin I, Steingart DA. Highly stretchable alkaline batteries based on an embedded conductive fabric. *Adv Mater*. 2012;24:5071-5076.

29. Yan C, Wang X, Cui M, et al. Stretchable silver-zinc batteries based on embedded nanowire elastic conductors. *Adv Energy Mater*. 2014;4:1301396.

30. Zamarayeva AM, Gaikwad AM, Deckman I, et al. Fabrication of a high-performance flexible silver-zinc wire battery. *Adv Electron Mater*. 2016;2:1500296.

31. Zeng YX, Zhang XY, Meng Y, et al. Achieving ultrahigh energy density and long durability in a flexible rechargeable quasi-solid-state Zn-MnO$_2$ battery. *Adv Mater*. 2017;29:7.

32. Huang Y, Liu J, Wang J, et al. An intrinsically self-healing NiCo||Zn rechargeable battery with a self-healable ferric-ion-crosslinking sodium polyacrylate hydrogel electrolyte. *Angew Chem Int Ed*. 2018;57:9810-9813.

33. Zhang N, Jia M, Dong Y, et al. Hydrated layered vanadium oxide as a highly reversible cathode for rechargeable aqueous zinc batteries. *Adv Funct Mater*. 2019;29:1807331.

34. Wang X, Li Y, Wang S, et al. 2D amorphous V$_2$O$_5$/graphene heterostructures for high-safety aqueous Zn-ion batteries with unprecedented capacity and ultrahigh rate capability. *Adv Energy Mater*. 2020;10:2000081.

35. Yu X, Fu Y, Cai X, et al. Flexible fiber-type zinc-carbon battery based on carbon fiber electrodes. *Nano Energy*. 2013;2:1242-1248.

36. Zhao J, Ren H, Liang Q, et al. High-performance flexible quasi-solid-state zinc-ion batteries with layer-expanded vanadium oxide cathode and zinc/stainless steel mesh composite anode. *Nano Energy*. 2019;62:94-102.

37. Berchmans S, Bandodkar AJ, Jia W, Ramírez J, Meng YS, Wang J. An epidermal alkaline rechargeable Ag-Zn printable tattoo battery for wearable electronics. *J Mater Chem A*. 2014;2:15788-15795.

38. Peng M, Yan K, Hu H, Shen D, Song W, Zou D. Efficient fiber shaped zinc bromide batteries and dye sensitized solar cells for flexible power sources. *J Mater Chem C*. 2015;3:2157-2165.

39. Shin J, You JM, Lee JZ, et al. Deposition of ZnO on bismuth species towards a rechargeable Zn-based aqueous battery. *Phys Chem Chem Phys*. 2016;18:26376-26382.

40. Lu K, Song B, Zhang Y, Ma H, Zhang J. Encapsulation of zinc hexacyanoferrate nanocubes with manganese oxide nanosheets for high-performance rechargeable zinc ion batteries. *J Mater Chem A*. 2017;5:23628-23633.

41. Lai W, Wang Y, Lei Z, et al. High performance, environmentally benign and integratable Zn//MnO$_2$ microbatteries. *J Mater Chem A*. 2018;6:3933-3940.

42. Li Q, Zhang Q, Liu C, et al. Anchoring V$_2$O$_5$ nanosheets on hierarchical titanium nitride nanowire arrays to form core-shell heterostructures as a superior cathode for high-performance wearable aqueous rechargeable zinc-ion batteries. *J Mater Chem A*. 2019;7:12997-13006.

43. Zamarayeva AM, Ostfeld AE, Wang M, et al. Flexible and stretchable power sources for wearable electronics. *Sci Adv*. 2017;3:e1602051.

44. Huang Y, Ip WS, Lau YY, et al. Weavable, conductive yarn-based NiCo//Zn textile battery with high energy density and rate capability. *ACS Nano*. 2017;11:8953-8961.

45. Wang K, Zhang X, Han J, et al. High-performance cable-type flexible rechargeable zn battery based on MnO$_2$@CNT fiber microelectrode. *ACS Appl Mater Interf*. 2018;10:24573-24582.

46. Pan Z, Yang J, Yang J, et al. Stitching of Zn$_3$(OH)$_2$V$_2$O$_7$·2H$_2$O 2D nanosheets by 1D carbon nanotubes boosts ultrahigh rate for wearable quasi-solid-state zinc-ion batteries. *ACS Nano*. 2020;14:842-853.

47. Wan F, Zhang LL, Dai X, Wang XY, Niu ZQ, Chen J. Aqueous rechargeable zinc/sodium vanadate batteries with enhanced performance from simultaneous insertion of dual carriers. *Nat Commun*. 2018;9:11.

48. Parker JF, Chervin CN, Pala IR, et al. Rechargeable nickel-3D zinc batteries: An energy-dense, safer alternative to lithium-ion. *Science*. 2017;356:414-417.

49. Takayuki S, Masakazu H, Takakazu Y. Zinc-manganese dioxide galvanic cell using zinc sulphate as electrolyte-rechargeability of the cell. *J Appl Electrochem*. 1988;18:521-526.

50. Li H, Liu Z, Liang G, et al. Waterproof and tailorable elastic rechargeable yarn zinc ion batteries by a cross-linked polyacrylamide electrolyte. *ACS Nano*. 2018;12:3140-3148.

51. Li M, Meng J, Li Q, et al. Finely crafted 3D electrodes for dendrite-free and high-performance flexible fiber-shaped Zn-Co batteries. *Adv Funct Mater*. 2018;28:1802016.

52. Guan Q, Li Y, Bi X, et al. Dendrite-free flexible fiber-shaped Zn battery with long cycle life in water and air. *Adv Energy Mater*. 2019;9:1901434.

53. Lee JM, Choi C, Kim JH, de Andrade MJ, Baughman RH, Kim SJ. Biscrolled carbon nanotube yarn structured silver-zinc battery. *Sci Rep*. 2018;8:11150.

54. Li C, Zhang Q, E S, et al. An ultra-high endurance and high-performance quasi-solid-state fiber-shaped Zn-Ag$_2$O battery to harvest wind energy. *J Mater Chem A*. 2019;7:2034-2040.

55. Zeng Y, Meng Y, Lai Z, et al. An ultrastable and high-performance flexible fiber-shaped Ni-Zn battery based on a Ni-NiO heterostructured nanosheet cathode. *Adv Mater*. 2017;29:1702698.

56. Li P, Jin Z, Xiao D. Three-dimensional nanotube-array anode enables a flexible Ni/Zn fibrous battery to ultrafast charge and discharge in seconds. *Energy Storage Mater*. 2018;12:232-240.

57. Wang Z, Ruan Z, Liu Z, et al. A flexible rechargeable zinc-ion wire-shaped battery with shape memory function. *J Mater Chem A*. 2018;6:8549-8557.

58. He B, Zhou ZY, Man P, et al. V$_2$O$_5$ nanosheets supported on 3D N-doped carbon nanowall arrays as an advanced cathode for high energy and high power fiber-shaped zinc-ion batteries. *J Mater Chem A*. 2019;7:12979-12986.

59. Wan F, Zhang L, Wang X, Bi S, Niu Z, Chen J. An aqueous rechargeable zinc-organic battery with hybrid mechanism. *Adv Funct Mater*. 2018;28:1804975.

60. Zhang Q, Li L, Li H, et al. Ultra-endurance coaxial-fiber stretchable sensing systems fully powered by sunlight. *Nano Energy*. 2019;60:267-274.

61. Zhang QC, Li CW, Li QL, et al. Flexible and high-voltage coaxial-fiber aqueous rechargeable zinc-ion battery. *Nano Lett*. 2019;19:4035-4042.

62. Ma L, Chen S, Long C, et al. Achieving high-voltage and high-capacity aqueous rechargeable zinc ion battery by incorporating two-species redox reaction. *Adv Energy Mater*. 2019;9:1902446.

63. Ho CC, Evans JW, Wright PK. Direct write dispenser printing of a zinc microbattery with an ionic liquid gel electrolyte. *J Micromech Microeng*. 2010;20:104009.

64. Gaikwad AM, Whiting GL, Steingart DA, Arias AC. Highly flexible, printed alkaline batteries based on mesh-embedded electrodes. *Adv Mater*. 2011;23:3251-3255.

65. Mo FNA, Li HF, Pei ZX, et al. A smart safe rechargeable zinc ion battery based on sol-gel transition electrolytes. *Sci Bull*. 2018;63:1077-1086.

66. Zhao T, Zhang G, Zhou F, Zhang S, Deng C. Toward tailorable Zn-ion textile batteries with high energy density and ultrafast capability: building high-performance textile electrode in 3D hierarchical branched design. *Small*. 2018;14: e1802320.

67. Mo F, Liang G, Meng Q, et al. A flexible rechargeable aqueous zinc manganese-dioxide battery working at −20°C. *Energ Environ Sci*. 2019;12:706-715.

68. Li H, Han C, Huang Y, et al. An extremely safe and wearable solid-state zinc ion battery based on a hierarchical structured polymer electrolyte. *Energ Environ Sci*. 2018;11:941-951.

69. Wang XW, Wang FX, Wang LY, et al. An aqueous rechargeable $Zn//Co_3O_4$ battery with high energy density and good cycling behavior. *Adv Mater*. 2016;28:4904-4911.

70. Huang Y, Li Z, Pei Z, et al. Solid-state rechargeable $Zn//NiCo$ and Zn-air batteries with ultralong lifetime and high capacity: the role of a sodium polyacrylate hydrogel electrolyte. *Adv Energy Mater*. 2018;8:1802288.

71. Ma L, Li N, Long C, et al. Achieving both high voltage and high capacity in aqueous zinc-ion battery for record high energy density. *Adv Funct Mater*. 2019;29:1906142.

72. Li H, Yang Q, Mo F, et al. $MoS_2$ nanosheets with expanded interlayer spacing for rechargeable aqueous Zn-ion batteries. *Energy Storage Mater*. 2019;19:94-101.

73. Yang Q, Mo F, Liu Z, et al. Activating C-coordinated iron of iron hexacyanoferrate for Zn hybrid-ion batteries with 10000-cycle lifespan and superior rate capability. *Adv Mater*. 2019; 31:1901521.

74. Kumar R, Shin J, Yin L, You J-M, Meng YS, Wang J. All-printed, stretchable $Zn-Ag_2O$ rechargeable battery via hyper-elastic binder for self-powering wearable electronics. *Adv Energy Mater*. 2017;7:1602096.

75. Zhao JW, Sonigara KK, Li JJ, et al. A smart flexible zinc battery with cooling recovery ability. *Angew Chem Int Ed*. 2017; 56:7871-7875.

76. Zhu H-W, Ge J, Peng Y-C, Zhao H-Y, Shi L-A, Yu S-H. Dip-coating processed sponge-based electrodes for stretchable $Zn-MnO_2$ batteries. *Nano Res*. 2018;11:1554-1562.

77. Zhu M, Wang Z, Li H, et al. Light-permeable, photo-luminescent microbatteries embedded in the color filter of a screen. *Energ Environ Sci*. 2018;11:2414-2422.

78. Shi J, Wang S, Chen X, et al. An ultrahigh energy density quasi-solid-state zinc ion microbattery with excellent flexibility and thermostability. *Adv Energy Mater*. 2019;9:1901957.

79. Lee JH, Lee HJ, Lim SY, et al. Stabilized octahedral frameworks in layered double hydroxides by solid-solution mixing of transition metals. *Adv Funct Mater*. 2017;27:1605225.

80. Zhang H, Wang R, Lin D, Zeng Y, Lu X. Ni-based nanostructures as high-performance cathodes for rechargeable Ni-Zn battery. *ChemNanoMat*. 2018;4:525-536.

81. Xiao H, Wu ZS, Chen L, et al. One-step device fabrication of phosphorene and graphene interdigital micro-supercapacitors with high energy density. *ACS Nano*. 2017;11:7284-7292.

82. Zheng S, Tang X, Wu ZS, et al. Arbitrary-shaped graphene-based planar sandwich supercapacitors on one substrate with enhanced flexibility and integration. *ACS Nano*. 2017;11:2171-2179.

83. Zheng S, Lei W, Qin J, et al. All-solid-state high-energy planar asymmetric supercapacitors based on all-in-one monolithic film using boron nitride nanosheets as separator. *Energy Storage Mater*. 2018;10:24-31.

84. Zhou F, Huang H, Xiao C, et al. Electrochemically scalable production of fluorine-modified graphene for flexible and high-energy ionogel-based microsupercapacitors. *J Am Chem Soc*. 2018;140:8198-8205.

85. Wu ZS, Zheng Y, Zheng S, et al. Stacked-layer heterostructure films of 2D thiophene nanosheets and graphene for high-rate all-solid-state pseudocapacitors with enhanced volumetric capacitance. *Adv Mater*. 2017;29:1602960.

86. Wang S, Wu ZS, Zheng S, et al. Scalable fabrication of photo-chemically reduced graphene-based monolithic micro-super-capacitors with superior energy and power densities. *ACS Nano*. 2017;11:4283-4291.

87. Gaikwad AM, Steingart DA, Nga Ng T, Schwartz DE, Whiting GL. A flexible high potential printed battery for powering printed electronics. *Appl Phys Lett*. 2013;102: 233302.

88. Kettlgruber G, Kaltenbrunner M, Siket CM, et al. Intrinsically stretchable and rechargeable batteries for self-powered stretchable electronics. *J Mater Chem A*. 2013;1:5505.

89. Pritesh Hiralal SI, Unalan HE, Matsumoto H, et al. Nano-material-enhanced all-solid flexible zinc-carbon batteries. *ACS Nano*. 2010;4:2730-2734.

90. Tan P, Chen B, Xu H, et al. $Co_3O_4$ nanosheets as active material for hybrid Zn batteries. *Small*. 2018;14:e1800225.

91. Wang F, Hu E, Sun W, et al. Rechargeable aqueous $Zn^{2+}$-battery with high power density and long cycle-life. *Energ Environ Sci*. 2018;11:3168-3175.

92. Yang Y, Tang Y, Fang G, et al. $Li^+$ intercalated $V_2O_5 \cdot nH_2O$ with enlarged layer spacing and fast ion diffusion as an aqueous zinc-ion battery cathode. *Energ Environ Sci*. 2018;11:3157-3162.

93. Zhu K, Wu T, Huang K. $NaCa_{0.6}V_6O_{16} \cdot 3H_2O$ as an ultra-stable cathode for Zn-ion batteries: the roles of pre-inserted dual-cations and structural water in $V_3O_8$ layer. *Adv Energy Mater*. 2019;9:1901968.

94. Xia C, Guo J, Li P, Zhang X, Alshareef HN. Highly stable aqueous zinc-ion storage using a layered calcium vanadium oxide bronze cathode. *Angew Chem Int Ed*. 2018;57:3943-3948.

95. Wu T, Zhu KY, Qin CY, Huang K. Unraveling the role of structural water in bilayer $V_2O_5$ during $Zn^{2+}$-intercalation: insights from DFT calculations. *J Mater Chem A*. 2019;7:5612-5620.

96. Liu C, Neale Z, Zheng J, et al. Expanded hydrated vanadate for high-performance aqueous zinc-ion batteries. *Energ Environ Sci*. 2019;12:2273-2285.

97. Dong LB, Yang W, Yang W, Li Y, Wu WJ, Wang GX. Multivalent metal ion hybrid capacitors: a review with a focus on zinc-ion hybrid capacitors. *J Mater Chem A*. 2019;7:13810-13832.

98. Sun GQ, Yang HS, Zhang GF, et al. A capacity recoverable zinc-ion micro-supercapacitor. *Energ Environ Sci*. 2018;11: 3367-3374.

99. Wang H, Wang M, Tang Y. A novel zinc-ion hybrid supercapacitor for long-life and low-cost energy storage applications. *Energy Storage Mater*. 2018;13:1-7.

100. An GH, Hong J, Pak S, et al. 2D metal Zn nanostructure electrodes for high-performance Zn ion supercapacitors. *Adv Energy Mater*. 2019;10:1902981.

101. Chen S, Ma L, Zhang K, Kamruzzaman M, Zhi C, Zapien JA. A flexible solid-state zinc ion hybrid supercapacitor based on co-polymer derived hollow carbon spheres. *J Mater Chem A*. 2019;7:7784-7790.

102. Wang N, Xin T, Zhao Y, Li Q, Hu M, Liu J. Boosting the capacitance of an aqueous zinc-ion hybrid energy storage device by using poly(3,3′-dihydroxybenzidine)-modified nanoporous carbon cathode. *ACS Sustain Chem Eng*. 2019;7: 14195-14202.

103. Ma XP, Cheng JY, Dong LB, et al. Multivalent ion storage towards high-performance aqueous zinc-ion hybrid supercapacitors. *Energy Storage Mater*. 2019;20:335-342.

104. Wang Q, Wang SL, Guo XH, et al. Mxene-reduced graphene oxide aerogel for aqueous zinc-ion hybrid supercapacitor with ultralong cycle life. *Adv Electron Mater*. 2019;5:1900537.

105. Wu S, Chen Y, Jiao T, et al. An aqueous Zn-ion hybrid supercapacitor with high energy density and ultrastability up to 80000 cycles. *Adv Energy Mater*. 2019;9:1902915.

106. Zhang H, Liu Q, Fang Y, et al. Boosting Zn-ion energy storage capability of hierarchically porous carbon by promoting chemical adsorption. *Adv Mater*. 2019;31:e1904948.

107. Zhang P, Li Y, Wang G, et al. Zn-ion hybrid micro-supercapacitors with ultrahigh areal energy density and long-term durability. *Adv Mater*. 2019;31:e1806005.

108. Dong L, Yang W, Yang W, et al. High-power and ultralong-life aqueous zinc-ion hybrid capacitors based on pseudocapacitive charge storage. *Nano-Micro Lett*. 2019;11:94.

109. Peng L, Peng X, Liu B, Wu C, Xie Y, Yu G. Ultrathin two-dimensional $MnO_2$/graphene hybrid nanostructures for high-performance, flexible planar supercapacitors. *Nano Lett*. 2013; 13:2151-2157.

110. Li P, Jin Z, Peng L, et al. Stretchable all-gel-state fiber-shaped supercapacitors enabled by macromolecularly interconnected 3D graphene/nanostructured conductive polymer hydrogels. *Adv Mater*. 2018;30:1800124.

111. Kim C, Ahn BY, Wei T-S, et al. High-power aqueous zinc-ion batteries for customized electronic devices. *ACS Nano*. 2018; 12:11838-11846.

112. Wang Z, Ruan Z, Ng WS, et al. Integrating a triboelectric nanogenerator and a zinc-ion battery on a designed flexible 3D spacer fabric. *Small Methods*. 2018;2:1800150.

113. Li H, Ding Y, Ha H, et al. An all-stretchable-component sodium-ion full battery. *Adv Mater*. 2017;29:1700898.

114. Wang Y, Ding Y, Guo X, Yu G. Conductive polymers for stretchable supercapacitors. *Nano Res*. 2019;12:1978-1987.

115. Li H, Zhang X, Zhao Z, Hu Z, Liu X, Yu G. Flexible sodium-ion based energy storage devices: recent progress and challenges. *Energy Storage Mater*. 2020;26:83-104.

116. Liu Z, Wang D, Tang Z, et al. A mechanically durable and device-level tough $Zn-MnO_2$ battery with high flexibility. *Energy Storage Mater*. 2019;23:636-645.

117. Li Y, Zhong C, Liu J, et al. Atomically thin mesoporous $Co_3O_4$ layers strongly coupled with N-rGO nanosheets as high-performance bifunctional catalysts for 1D knittable zinc-air batteries. *Adv Mater*. 2018;30:1703657.

118. Yang H, Chang Z, Qiao Y, et al. Constructing a super-saturated electrolyte front surface for stable rechargeable aqueous zinc batteries. *Angew Chem Ed Int*. 2020;59:9377-9381. https:// doi.org/10.1002/anie.202001844.

119. Zhang Q, Luan J, Tang Y, Ji X, Wang HY. Interfacial design of dendrite-free zinc anodes for aqueous zinc-ion batteries. *Angew Chem Int Ed*. 2020. https://doi.org/10.1002/anie. 202000162.

120. Xie X, Liang S, Gao J, et al. Manipulating the ion-transfer kinetics and interface stability for high-performance zinc metal anodes. *Energ Environ Sci*. 2020;13:503-510.

121. Xiong T, Yu ZG, Wu H, et al. Defect engineering of oxygen-deficient manganese oxide to achieve high-performing aqueous zinc ion battery. *Adv Energy Mater*. 2019;9:1803815.

122. Nam KW, Park SS, Dos Reis R, et al. Conductive 2D metal-organic framework for high-performance cathodes in aqueous rechargeable zinc batteries. *Nat Commun*. 2019;10:4948.

123. Tang B, Shan L, Liang S, Zhou J. Issues and opportunities facing aqueous zinc-ion batteries. *Energ Environ Sci*. 2019;12: 3288-3304.

124. Huang J, Guo Z, Ma Y, Bin D, Wang Y, Xia Y. Recent progress of rechargeable batteries using mild aqueous electrolytes. *Small Methods*. 2018;3:1800272.

125. Wang F, Borodin O, Gao T, et al. Highly reversible zinc metal anode for aqueous batteries. *Nat Mater*. 2018;17:543-549.

126. Sun W, Wang F, Hou S, et al. $Zn/MnO_2$ battery chemistry with $H^+$ and $Zn^{2+}$ coinsertion. *J Am Chem Soc*. 2017;139: 9775-9778.

127. Wu K, Huang J, Yi J, et al. Recent advances in polymer electrolytes for zinc ion batteries: mechanisms, properties, and perspectives. *Adv Energy Mater*. 2020;10:1903977.

128. Wang D, Han C, Mo F, et al. Energy density issues of flexible energy storage devices. *Energy Storage Mater*. 2020;28:264-292.

129. Zheng S, Huang H, Dong Y, et al. Ionogel-based sodium ion micro-batteries with a 3D Na-ion diffusion mechanism enable ultrahigh rate capability. *Energ Environ Sci*. 2020;13:821-829.

130. Li H, Xu M, Zhang Z, Lai Y, Ma J. Engineering of polyanion type cathode materials for sodium-ion batteries: toward higher energy/power density. *Adv Funct Mater*. 2020;2000473. https://doi.org/10.1002/adfm.202000473.

131. Li H, Tang Z, Liu Z, Zhi C. Evaluating flexibility and wearability of flexible energy storage devices. *Joule*. 2019;3:613-619.

132. Gaikwad AM, Arias AC, Steingart DA. Recent progress on printed flexible batteries: mechanical challenges, printing technologies, and future prospects. *Energ Technol*. 2015;3: 305-328.

133. Ma L, Chen S, Li N, et al. Hydrogen-free and dendrite-free all-solid-state Zn-ion batteries. *Adv Mater*. 2020;32:e1908121.

## AUTHOR BIOGRAPHIES

**Xiao Wang** obtained BS degree in material chemistry from Shandong Agricultural University in 2016. She is pursuing the PhD degree from Dalian Institute of Chemical Physics (DICP), Chinese Academy of Sciences (CAS), under the supervision of Prof. Zhong-Shuai Wu. Her research interests focus on graphene and 2D materials, flexible and planar electrochemical energy storage devices.

**Zhong-Shuai Wu** received his PhD from the Institute for Metal Research, CAS in 2011, and worked as a postdoctoral fellow at the Max Planck Institute for Polymer Research in Mainz, Germany from 2011 to 2015. Subsequently, Dr Wu became a full professor at DICP, CAS, and was promoted in 2018 as a DICP chair professor. He is a Group leader of 2D Materials Chemistry & Energy Applications, affiliated with State Key Laboratory of Catalysis. Currently, Prof. Wu's research interests include graphene and 2D materials, surface electrochemistry and nanoelectrochemistry, microscale electrochemical energy storage devices, supercapacitors, batteries, and catalysis. He is a recipient of the National Natural Science Award (second class, 2017), the 2018 and 2019 High Cited Researchers (Clarivate Analytics), and the Fellow of the Royal Society of Chemistry. He is an editor of *Applied Surface Science*, section editor of *Journal of Energy Chemistry*, and editorial board of *Energy Storage Materials*, *Journal of Physics: Energy, and Physics*.